The influence of coral reef spur and groove morphology on wave energy dissipation and wave overtopping under future climate change scenarios

Lachlan A Perris[1], Tristan Benjamin Salles[1], Thomas E Fellowes[1], Stephanie Jane Duce[2], Jody M Webster[1], and Ana Vila-Concejo[1]

[1]University of Sydney
[2]James Cook University

September 18, 2023

Abstract

Coral reefs protect coastlines from inundation and flooding, servicing over 200 million people globally. Wave transformation has previously been studied on coral reef flats with limited focus on forereef zones where wave transformation is greatest during high-energy conditions. This study investigates the role of forereef spur and groove (SaG) morphology on wave energy dissipation and overtopping on coral reefs. Using XBeach on LiDAR-derived bathymetry, we reproduced dissipation rates comparable to SaG field studies. Our results emphasize accurate bathymetries' role in forereef wave energy dissipation models by including morphological features (e.g., groove sinuosity, irregular forereef slopes) that control the mode of wave energy dissipation (frictional and breaking). We then investigated changes to wave energy dissipation and wave overtopping based on IPCC AR5 low and high emission scenarios (RCP2.6 and RCP8.5) and a total disaster scenario (TD) for the year 2100 considering changes to SaG morphology, wave power and relative sea-level rise. For RCP2.6, an increase in wave heights of 0.8 m and an increase in water level of 0.3 m resulted in a two-fold increase in dissipation rates. For RCP8.5 and TD, with no increase in incident wave height, dissipation rates were 29% and 395% lower than RCP2.6. This resulted in increased overtopping at the reef crest by 1.8 m and 2.7 m for RCP8.5 and TD scenarios, respectively, when compared to RCP2.6. Decreased dissipation rates and increased wave overtopping in forecasted climate conditions suggest the need for strategies to promote coral growth to facilitate high dissipation rates in the future.

1 **The influence of coral reef spur and groove morphology on wave energy dissipation and**
2 **wave overtopping under future climate change scenarios**

3

4 **Lachlan Perris[1,*], Tristan Salles [1], Thomas E Fellowes[1], Stephanie Duce[2], Jody Webster[1], Ana Vila-**
5 **Concejo[1]**

6 [1] Geocoastal Research Group and Marine Studies Institute, School of Geosciences, The University of
7 Sydney, NSW, 2006, Australia

8 [2] College of Science and Engineering, James Cook University, Bebegu Yumba Campus, Townsville,
9 Queensland 4811, Australia

10 * Corresponding Author, lachlan.perris@sydney.edu.au

11

12 Key Points:

13 •   Accurate bathymetries (<1 m) in forereef wave energy dissipation models highlight
14   previously overlooked features of the forereef, including spurs and grooves (SaG).
15 •   SaG influence forereef wave energy dissipation and this influence can be related to the
16   SaG morphology.
17 •   Future climate change projections modify dissipation rates by shifting the dominant
18   mode of dissipation (from bed friction to wave breaking) leading to an increase wave
19   overtopping on forereefs.

20

Abstract

22 Coral reefs protect coastlines from inundation and flooding, servicing over 200 million people

23 globally. Wave transformation has previously been studied on coral reef flats with limited focus on

24 forereef zones where wave transformation is greatest during high-energy conditions. This study

25 investigates the role of forereef spur and groove (SaG) morphology on wave energy dissipation and

26 overtopping on coral reefs. Using XBeach on LiDAR-derived bathymetry, we reproduced dissipation

27 rates comparable to SaG field studies under present-day conditions. Our results highlight the

28 benefits of accurate bathymetries in forereef wave energy dissipation models, as they incorporate

29 critical morphological features (e.g., groove sinuosity, irregular forereef slopes) that exert control

30 over mode of wave energy dissipation (frictional and breaking). We then investigated changes to

31 wave energy dissipation and wave overtopping based on IPCC AR5 low and high emission scenarios

32   (RCP2.6 and RCP8.5) and a total disaster scenario (TD) for the year 2100 considering changes to SaG

33   morphology, wave power and relative sea-level rise. For RCP2.6, an increase in wave heights of 0.8

34   m and an increase in water level of 0.3 m resulted in a two-fold increase in dissipation rates. For

35   RCP8.5 and TD, with no increase in incident wave height, dissipation rates were 29% and 395% lower

36   than RCP2.6. This resulted in increased overtopping at the reef crest by 1.8 m and 2.7 m for RCP8.5

37   and TD scenarios, respectively, when compared to RCP2.6. Decreased dissipation rates and

38   increased wave overtopping in forecasted climate conditions suggest the need for strategies to

39   promote coral growth to facilitate high dissipation rates in the future. The results from our novel

40   modelling approach have implications for the future habitability of exposed reef-lined coasts due to

41   increased exposure to coastal flooding and island inundation.

Plain language summary

43   Coral reefs are essential for protecting coastlines from floods and waves, benefiting over 200 million

44   people worldwide. We studied how waves change as they approach coral reefs, focusing on the

45   forereef zone where wave transformation is most significant during high-energy conditions. The

46   shape of the forereef, specifically the spur and groove (SaG) morphology, plays a crucial role in how

47   much wave energy is dissipated and how much water spills over the reef.

48   Using a digital representation of waves over accurate reef shapes (known at bathymetry), we

49   simulated wave dissipation rates comparable to real-world SaG studies. Our findings emphasize the

50   importance of accurate representations of forereef shapes in models to predict wave energy

51   dissipation, as they consider critical features such as SaG which affect how waves transform and lose

52   energy.

53   Next, we investigated how wave energy dissipation and overtopping might change under different

54   future climate scenarios. We considered low and high emission scenarios (RCP2.6 and RCP8.5) from

55   the IPCC AR5 report and a total disaster scenario (TD) for the year 2100, factoring in changes to

56   forereef elevation, wave power, and sea-level rise.

57   Under the low emission scenario (RCP2.6), with a slight increase in wave heights and water levels,

58   we observed a doubling of wave energy dissipation rates. However, under the high emission

59   scenario (RCP8.5) and the total disaster scenario (TD), dissipation rates decreased significantly

60   compared to RCP2.6, resulting in more water moving over the reef crest during storms. This suggests

61   that future climate conditions may lead to increased flooding and inundation on reef-lined coasts,

62   putting communities at risk.

63   In summary, our study highlights the benefits of using accurate reef shapes in simulating wave

64   energy dissipation on coral reefs. Accurate bathymetries can incorporate features such as spurs and

65   grooves of different shapes, which modify wave dissipation. Wave energy dissipation changes when

66   climate change projections are incorporated into the simulations leading to an increase in energy

67   passing over the forereef.

1. Introduction

68

69   Coral reefs provide many ecosystem services including coastal hazard protection from ocean waves,

70   with over 200 million people worldwide depending on the stability of this service (Ferrario et al.,

71   2014). Coral reefs are topographically complex structures which contribute to the frictional

72   dissipation of waves, however this has been studied in greater details on the reef crest and reef flat

73   (Ferrario et al., 2014; Monismith et al., 2015; Péquignet et al., 2014; Yao et al., 2020) than on the

74   high-energy environments of the forereef slope (Acevedo-Ramirez et al., 2021; Duce et al., 2014,

75   2016, 2022; Monismith et al., 2013; Sheppard, 1981). Yet, wave breaking on the forereef slope is the

76   dominant form of wave energy dissipation under high-energy conditions (Osorio-Cano et al. 2018)

77   suggesting that it is a critical region for coastal protection (Quataert et al. 2015a). High dissipation

78   rates on the forereef are controlled by forereef morphology such as spurs and grooves (SaG)

79   (Monismith et al., 2013; Osorio-Cano et al. 2018).

80   SaG are shore-normal elongate ridges (spur) and troughs (groove) on the forereef slopes of many

81   coral reefs (Duce et al., 2016). Their size, spacing and orientation are typically aligned with incident

82   waves and consequently the morphometric classification of SaG (Duce et al., 2016) reflects the

83   influence of waves in their formation (Table 1). High energy forereefs feature more defined SaG than

84   low-energy ones (Duce et al., 2016; Rogers et al., 2013). Recent research shows high-relief (up to 10

85   m) spurs in the Mexican Caribbean have a large influence over wave transformation, with dissipation

86   in the SaG zone contributing a 35% in wave energy flux. Wave energy flux on the forereef occurs

87   mostly in the sea-swell frequency band (> 0.04 Hz). While infragravity waves (0.004-0.04 Hz) are

88   important to wave transformation over reef flats and in lagoons (Cheriton et al. 2016), field

89   measurements of waves over SaG have shown negligible energy in the infragravity bands (Duce et al.

90   2022). A recent investigation into SaG morphology demonstrates that SaG are not optimised to

91   maximise wave energy dissipation, with their morphology dissipating energy while allowing energy

92   propagation (and water, nutrients, and oxygen) to facilitate coral growth in the lagoon (Johannsen et

93   al., in review). Further field investigations are required but have been limited by the difficulty of

94   accessing highly exposed and turbulent forereef slopes (Sheppard 1981; Sous et al. 2022).

95   SaG morphologies have been overlooked in both physical (e.g., Buckley et al., 2016) and numerical

96   models (e.g. Baldock et al., 2020; Monismith et al., 2013; Osorio-Cano et al., 2018) of forereef wave

97   attenuation. For instance, numerical models that include SaG morphologies typically use idealised

98   bathymetries (e.g. da Silva et al., 2020; Rogers et al., 2013) with simplified morphologies that

99   overlook the irregularity and diversity of SaG. Consequently, the impact of SaG morphologies (Table

100   1) on wave attenuation is poorly understood (Duce et al., 2022; Monismith et al., 2013; da Silva et

101   al., 2020).

102   Table 1: Morphological categorisation of SaG (Duce et al., 2016).

Deep and Disconnected (DaD)	Grooves are disconnected from the reef crest and appear in deeper water (>5.5m) with limited hydrodynamic energy
Exposed to wave energy (EWE)	This morphology is heavily governed by the wave climate. Grooves are oriented perpendicular to incoming wave crests.
Log and protected (LaP)	Grooves are longer (>50m) and wider than more exposed grooves
Short and protected (SaP)	These grooves are narrower and shorter than Class 3.

103

104   Studies have shown that forereef morphologies including SaG will be impacted by climate change

105   (Castillo et al., 2012; De'Ath et al., 2012; Hughes et al., 2018) likely resulting in reduced coastal

106   protection (Baldock et al., 2014; Ferrario et al., 2014; Quataert et al., 2015; Sheppard et al., 2005)

107   and increased wave overtopping (Amores et al. 2022; Beetham and Kench 2018). Most notably, a

108   loss of structural complexity (roughness) in forereefs will reduce bed friction impacting wave

109   attenuation (Baldock et al., 2014; Harris et al., 2018; Monismith et al., 2015; Rogers et al., 2016).

110   These impacts are exacerbated by relative sea-level rise, changes in regional wave power (Meucci et

111   al., 2020; Reguero et al., 2019) and modification and intensification of storm climates (Knutson et al.,

112   2015) which all modify wave transformation processes on forereefs.

113   The overall aim of this paper is to provide understanding of present day and forecasted wave

114   attenuation by SaG on coral reefs. Both of which are critical for coral reef management plans and

115   climate change adaptation strategies. To achieve this, we first identify the benefits of high-resolution

116   LiDAR-derived bathymetries in numerical wave models. Then we employ these models to determine

117   how SaG of different morphological class affect the dissipation of wave energy. Finally, we

118   investigate the effects of climate change on wave energy dissipation over SaG.

2. Methods

2.1 Study Site

One Tree Reef (OTR) (23°30'S, 152°06'E) is located 84 km offshore of the NE Australian mainland in the Capricorn Bunker Group, in the southern Great Barrier Reef (GBR) (Figure 1a). OTR is a lagoonal platform reef with semi-diurnal tides with a mean spring tidal range of 3 m. The entire forereef of OTR features SaG (Duce et al., 2016). The mean significant offshore wave height, $H_{s,mean}$ of 1.7 m (Smith et al., 2022) is typically generated from persistent SE trade winds that dominate the Coral Sea for over 70% of the year (Jell and Webb, 2012). Consequently, the south-eastern forereef is the most exposed to ocean swells (Figure 1b). We considered two study sites featuring SaGs of varying morphological class (Table 1) on the eastern and southern side of OTR (henceforth labelled OE and OS respectively) (Figure 1b, Table 1).
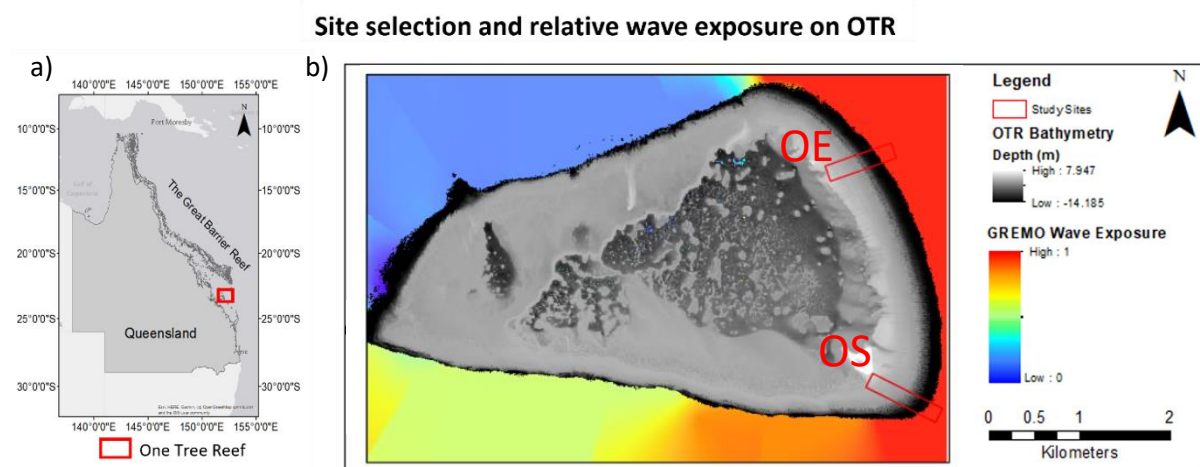

Figure 1: a) One Tree Reef (OTR) in the Southern Great Barrier Reef, and b) Study site locations for OTR East (OE) and OTR South (OS) and relative wave exposure (Pepper and Puotinen 2009).

2.2 SaG morphometric analysis

We determined morphometric parameters for SAG in the two study sites including length, depth, width, and others (Table 2) from analysis of LiDAR derived bathymetry and used them to classify the SAG following the categorical framework of Duce et al. (2016) (Table 1).

137   Table 2: Morphometric parameters of SaG adapted from Duce et al. (2016).

Morphometric parameter	Method
Length (L)	Path distance along the groove (m)
Depth (D)	The vertical distance between the lowest point in the groove and the highest point on the neighbouring spur is calculated at four depths below sea level (-2, -4, -6, and -8 meters).
Width (W)	Groove width is measured as the horizontal distance between its walls at half the depth, along isobaths of -2, -4, -6 and -8 m.
Orientation (θ)	Azimuth of straight line between maximum onshore and offshore extents of groove
Sinuosity (S)	Ratio of straight-line distance (D) to path length (L) such that: $S = D/L$
Wavelength (γ_{sag})	The horizontal distance between the highest points of adjacent ridges, parallel to isobaths, measured at depths of -2, -4, -6, and -8 meters below mean sea level.

138

2.3. Wave transformation modelling (XBeach)

140   We used XBeach (Roelvink et al., 2015) in Surf Beat mode to understand hydrodynamics and wave

141   attenuation over SaG because it has been extensively validated on complex coral reef bathymetries

142   (Harris et al., 2018; Lashley et al., 2018; Quataert et al., 2015, 2020; da Silva et al., 2020).

2.3.1 Bathymetric Grids

144   We merged data from a 0.5 m resolution Airborne LiDAR survey (Harris et al., 2023) to a depth of 14

145   m, and a 30 m resolution bathymetry survey (Beaman, 2017) to a maximum depth of 20 m (Figure

146   2). This maximum depth was selected to capture all depth-limited wave breaking within the model

147   and was based on historical wave heights for OTR considering,

Eq. 1   7

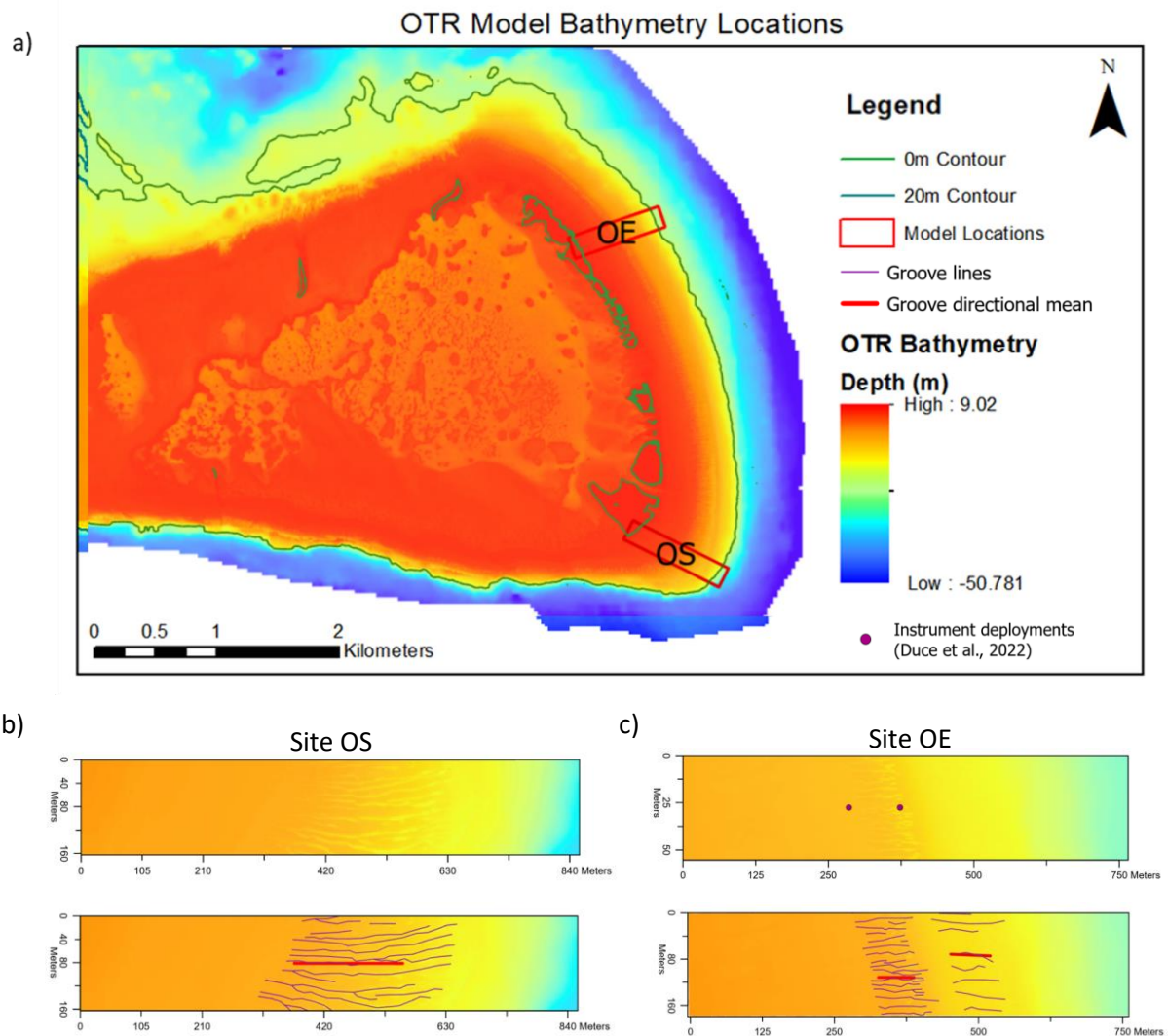148
$$H_{max} = \gamma \cdot (h + \delta H_{rms})$$

149   where, γ is the breaker index, δH_{rms} is some fraction δ of the root mean square of the wave height.

150   The breaker index was held constant across the reef at $\gamma = 0.55$, reflecting the conservative

151   estimation ($\gamma = 0.55$) of (Duce et al., 2022) and within the ranges determined by Harris et al. (2018).

152

153   *Figure 2: a) The bathymetric grids used in wave models from two study sites on the eastern (OE) and*

154   *southern (OS) exposed forereefs of on One Tree Island. Grooves are shown in purple with the*

155   *directional mean of SaG shown in red.*

156   The outer boundaries of the bathymetric grids were oriented to align mean groove headings with

157   incident waves (Figure 2b and c), following field observations (Duce et al., 2014; Munk and Sargent,

158   1948; Shinn, 1963) and other wave transformation models constructed over SaG (Rogers et al., 2013;

159   da Silva et al., 2020) (Figure 2b). Offshore boundaries were set beyond the maximum breaker depth

160   for modelled wave heights (20 m: Eq. 1) and the onshore boundaries at present-day 0 m MSL

161   contour (Figure 2b, c). Consequently, grids for each site are of different length and width (Figure 2b).

162   ## 2.3.2 Climate change projections

163   We considered four climate change scenarios projected for the year 2100 including critical climate

164   impacts to wave energy dissipation on coral reefs: sea-level change, reef health and wave energy

165   conditions. The climate change scenarios are based on IPCC AR5 and include (1) the *present-day*

166   scenario considering no change to current environmental factors, (2) the *low* (RCP 2.6) and (3) *high*

167   (RCP8.5) emission scenarios from the AR5 IPCC report (Shukla et al., 2019), and (4) a *total disaster*

168   (TD) scenario included to represent a high carbon future.

169   *2.3.2.1 Changes to Sea Level*
170   We used IPCC AR5 sea-level rise (SLR) rate of 3 mm/yr (Shukla et al., 2019). Under the *low* and *high*

171   emission scenarios (RCP2.6 and RCP8.5) SLR is expected to reach up to 10-20 mm/yr. Subsequently,

172   we have included SLR of 0.43 m (RCP2.6) and 0.84 m (RCP8.5) for the year 2100 (Shukla et al., 2019).

173   Human stressors (e.g., infrastructure development and human-induced habitat degradation) are also

174   likely to contribute to increases in local SLR (Shukla et al., 2019). An additional 1 m of eustatic SLR

175   was included for our *total disaster* (TD) scenario to reflect significant changes to climate conditions

176   and non-climatic anthropogenic stressors (Shukla et al., 2019) (Table 3). The total sea-level increase

177   in each of the models (Table 3) was determined by the sum of eustatic and local sea-level changes,

178   and the vertical accretion and erosion of the reefs.

179   *2.3.2.2 Reef Morphological Changes*
180   Reef morphological changes have been simplified into three key characteristics, reef vertical

181   accretion, erosion, and structural complexity. A forecasted vertical accretion rate of 2 mm/yr was

182   used based on field measurements from coral reef cores from across the GBR (Dechnik et al., 2015;

183   Sanborn et al., 2020), Western Australia (Perry et al., 2018), Tahiti (Buddemeier and Smith, 1988),

184   the Maldives (Kench et al., 2022), Indo-Pacific averages compiled by Montaggioni (2005) and the

185   Solomon Islands (Saunders et al., 2016). Alternatively, erosion of forereefs can occur due to the

186   physical removal of coral and framework by storms and high wave energy (Madin and Connolly,

187   2006). This is most evident on degraded coral reefs where erosion has been observed at 6 mm/yr

188   (Eakin, 1996; Sheppard et al., 2005). We used a conservative estimate of 2.6 mm/yr (0.2 m by 2100)

189   of reef erosion for RCP 8.5 and a maximum of 6.4 mm/yr (0.5 m by 2100) of erosion under a TD

190   scenario, modelled as a uniform decrease in elevation over the simulated domain. The resulting sea

191   level was determined by combining projected rates of SLR with erosion and accretion values for each

192   scenario (Table 3).

193   To simulate a loss in forereef structural complexity, we altered the dimensionless wave friction

194   factor (f_w) to replicate changes to coral structural complexity. In our study, f_w were linearly

195   interpolated between $f_w = 0.9$ (healthy reef) to $f_w = 0.1$ (degraded or smoothed reef). For the *total*

196   *disaster* (TD) scenario, which represents a degraded reef and a shift to a carbonate sand substrate

197   we used $f_w = 0.01$ (Smyth and Hay, 2002) (Table 3).

2.3.3 Wave Input Parameters

199   Mean offshore wave conditions were determined by satellite altimeter observations over 30 years

200   (1985–2015) using RADWave (Smith et al., 2020) (Table 3). A small region (0.6° x 0.4°) representing

201   dense altimeter data tracks was identified on the eastern, exposed side of OTR (Figure S1). We

202   determined site-specific model input wave heights (H_{model}) by combining offshore wave conditions

203   with a relative wave exposure model, GREMO (GIS-based generic model for estimating relative wave

204   exposure; see Figure 1b) following Pepper and Puotinen (2009),

$$H_{model} = K_r \; H_{offshore} \tag{1}$$

206   where, $H_{offshore}$ is the offshore wave height obtained from RADWave (Figure 1b and Figure S1) and

207   K_r is the relative exposure coefficient, normalised between 1 (most exposed) and 0 (least exposed).

208   Finally, altimeter wave heights were compared to measured waves at the northern forereef at OTR

209   (Duce et al., 2022).

2.3.4 Changes to wave climate

211   We increased offshore model wave heights ($H_{offshore}$) for future climate change scenarios (Table 3)

212   with wave periods (T_{model}) determined for a fully developed sea-state from the Joint North Sea Wave

213   Project (JONSWAP) spectrum (Young, 1992). Storm waves were calculated from the maximum wave

214   height observed in RADWave altimeter data. The final model wave heights were dependent on

215   forereef location and relative exposure to wave energy determined by Eq. 1.

216   *Table 3: Model input parameters are presented for three study sites, two wave conditions and four*

217   *forecasted climate outcomes for the year 2100. A total of 16 unique models were run.*

Site	Climate scenario	Wave Condition	$H_{offshore}$ (m)	Exposure Factor	H model (m)	T_{model} (s)	Friction factor	SLR (m)	Vertical Accretion (m)	Reef erosion (m)	Total change in MSL (m)
OS	Present day	Mean	1.34	0.985	1.3	5.74	0.9	0	0	0	0
	RCP 2.6		2.14				0.54	0.43	0.16	0	0.3
	RCP 8.5		2.14		2.1	7.26	0.1	0.84	0.1	0.2	0.99
	TD		2.14				0.01	1.84	0	0.5	2.34
	Present day	Storm	4.8		4.7	10.87	0.9	0	0	0	0
	RCP 2.6						0.54	0.43	0.16	0	0.3
	RCP 8.5		5.6		5.5	11.74	0.1	0.84	0.1	0.2	0.99
	TD						0.01	1.84	0	0.5	2.34
OE	Present day	Mean	1.34	0.9042	1.2	5.5	0.9	0	0	0	0
	RCP 2.6		2.14				0.54	0.43	0.16	0	0.3
	RCP 8.5		2.14		1.9	6.96	0.1	0.85	0.1	0.2	0.99
	TD		2.14				0.01	1.84	0	0.5	2.34
	Present day	Storm	4.8		4.3	10.42	0.9	0	0	0	0
	RCP 2.6		5.6				0.54	0.43	0.16	0	0.3
	RCP 8.5		5.6		5.1	11.25	0.1	0.84	0.1	0.2	0.99
	TD		5.6				0.01	1.84	0	0.5	2.34

218

219   2.3.5 XBeach model outputs

220   Each model was run for a total of 300 seconds, and we analysed the outputs of Xbeach for water

221   surface elevation (zs), total dissipation rate (D), and dissipation rate due to bed friction (D_f) to

222   obtain wave energy dissipation rates and wave overtopping. Total dissipation was used to compare

223   Xbeach results with field measurements and to determine dissipation by breaking (D_b) such that

224    $D_b = D - D_f$. As models are two-dimensional (x, y spatial domains) and evolve through time (t), we

225   calculated mean and peak dissipation rates across t and x domains for the entire bathymetric grid.

226   Mean dissipation rates were also taken between two points where hydrodynamic data sampled by

227   Duce et al. (2022). Wave overtopping was calculated as the difference between the initial water level

228   at the reef crest and the maximum water level at the reef crest during each model run.

3. Results

3.1 SaG morphometric analysis

231   SaG morphometrics were quantified for 123 grooves across the two study sites (Table 3). Grooves at

232   the southern site (OS) were on average 3 times longer, 1.4 times deeper and 1.3 times wider than

233   those at the eastern site (OE) (Table 3). Using the morphometric classification of Duce et al. (2016),

234   the exposed to wave energy (EWE) grooves were the most common across three of the four sites

235   (100 of 123 SaG) (Table 3). Deep and disconnected (DaD) grooves were present on the lower

236   forereef platform of site OE.

237   *Table 4: Morphometric parameters and classes of SaG at two study sites.*

	Mean SaG Morphometric Parameters					Quantity of SaG Classes by Site			
Site	Length (m)	Sinuosity	Orientation (Deg)	Depth (m)	Width (m)	DaD	EWE	LaP	SaP

OS (south)	187.12	0.99	116.73	1.95	4.02	0	40	0	0
OE (east)	63.18	0.99	71.5	1.38	3.12	23	60	0	0

3.2 Wave transformation over LiDAR derived bathymetry

The peak dissipation rates under present day conditions, taken as the maximum dissipation across all axes (x, y, t), were 463.9 and 946.3 W/m^2 at sites OE and OS respectively (Figure 4). Wave energy dissipation due to bed friction was dominant in present day scenarios over dissipation due to wave breaking (Figure 4b and d). Between the two locations of field measurements conducted by Duce et al., (2022) (Figure 2c) the mean dissipation rate was 10.6 W/m^2, the maximum dissipation rate of 463.9 W/m^2 occurred during this zone. Wave energy dissipation by bed friction contributed 78% of energy at the site OE before waves reached the reef crest, 67% at site OS in the upper forereef slope. The maximum wave energy dissipation due to wave breaking constituted 22%, and 32% of total dissipation at site OE and OS respectively (Figure 4b, d).
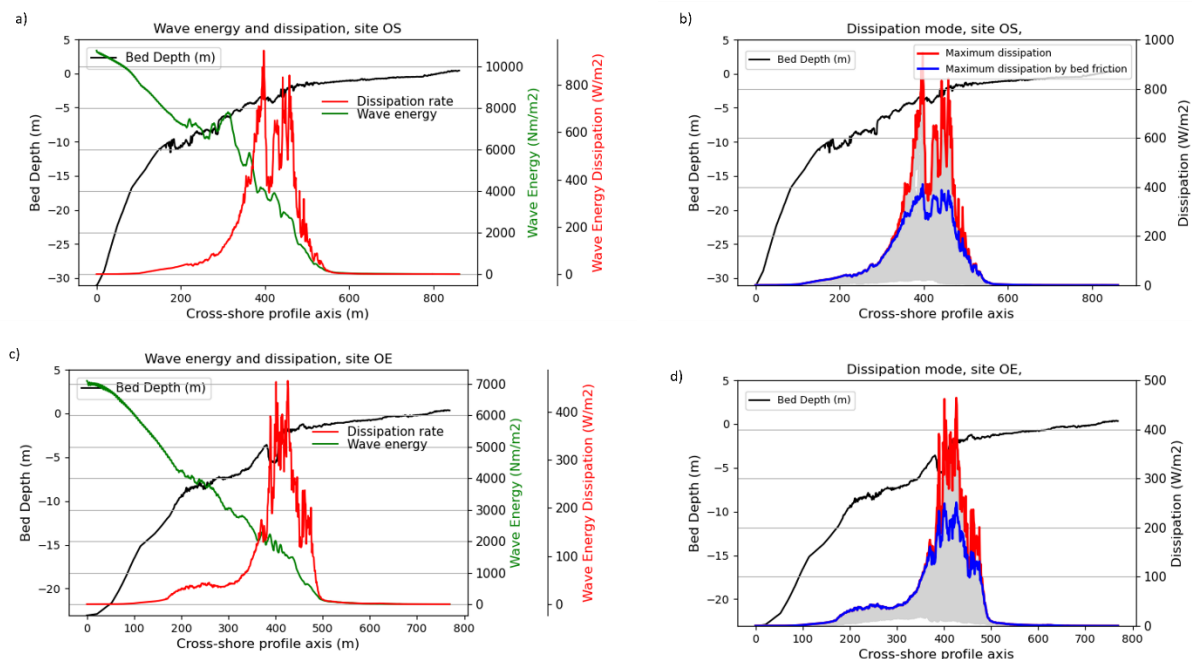
250   *Figure 4: Wave energy (green) and maximum wave energy dissipation at site OS (a) and site OE (c).*

251   *Maximum dissipation and maximum dissipation by bed friction (blue) for site OS (b) and site OE (d).*

252   *Note different scale bars are used for each site.*

3.3 Wave transformation under future climate change projections

254   Wave transformation was found to vary greatly among models depending on climate change

255   scenario, SaG morphometrics, and wave exposure. The largest influence on wave energy dissipation

256   across the two sites was the reduction of the bed friction factor (f_w), increased water depth, and

257   increased wave height. Total wave energy dissipation and dissipation due to bed friction changed at

258   both sites for all future climate scenarios (Table 3).

259   Mean and peak dissipation rates were computed for each site across all three climate scenarios

260   (Table 3, Figure 5). When comparing dissipation rates from present day to RCP2.6 for the year 2100,

261   mean dissipation increased by 187% at site OS (4.4 to 12.5 W/m^2) and maximum dissipation

262   increased by 59.7% (946.3 to 1511.4 W/m^2) (Figure 5a and b). At site OE, mean dissipation rate

263   increased by 208.6% (2.5 to 7.8 W/m^2) and maximum dissipation increased by 217.7% (463.9 to

264   1473.4 W/m^2) (Figure 5d and e).

265   When comparing RCP2.6 to RCP8.5 we found a decrease in mean dissipation across site OS of 18.1%

266   (12.5 to 10.6 W/m^2) and an increased in the max dissipation rate of 23.2% (1511.4 to 1966.9 W/m^2).

267   Site OE retained at high mean dissipation rate from RCP2.6 to RCP8.5, increasing a further 11.7%

268   (7.78 to 8.81 W/m^2) and an increase of 19.3% to peak dissipation rate (1473.42 to 1824.70 W/m^2).

269   When comparing to RCP8.5, the TD scenario, mean dissipation rates decreased by 66.2% (10.61 to

270   3.58 W/m^2) at site OS and a decrease in peak dissipation of 31.8% (1966.89 to 1340.93 W/m^2)

271   (Figure 4b and c). At site OE, mean dissipation decreased by 86.2% (8.81 to 1.21 W/m^2) and peak

272   dissipation rate decreased by 75.4% (1824.7 to 448.24 W/m^2) (Figure 5e and f).
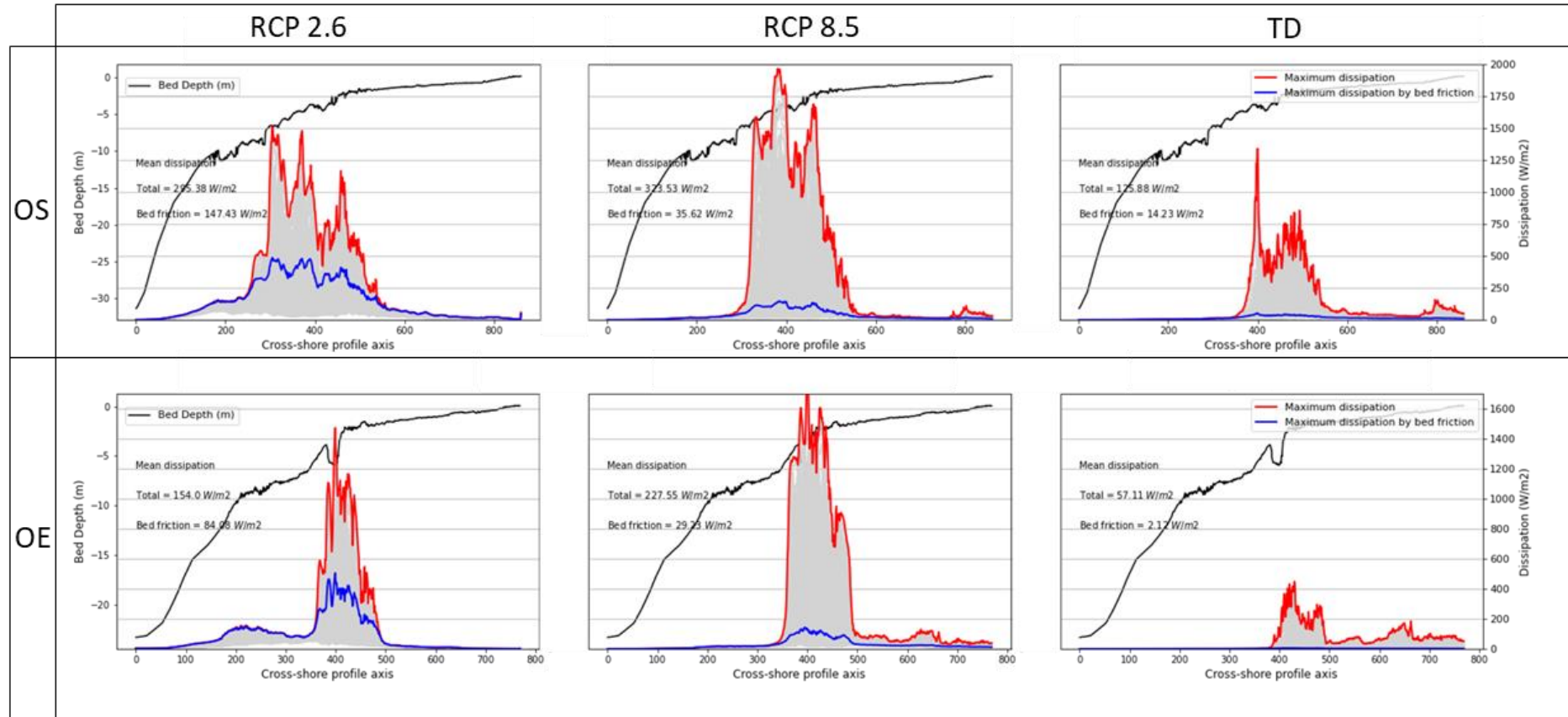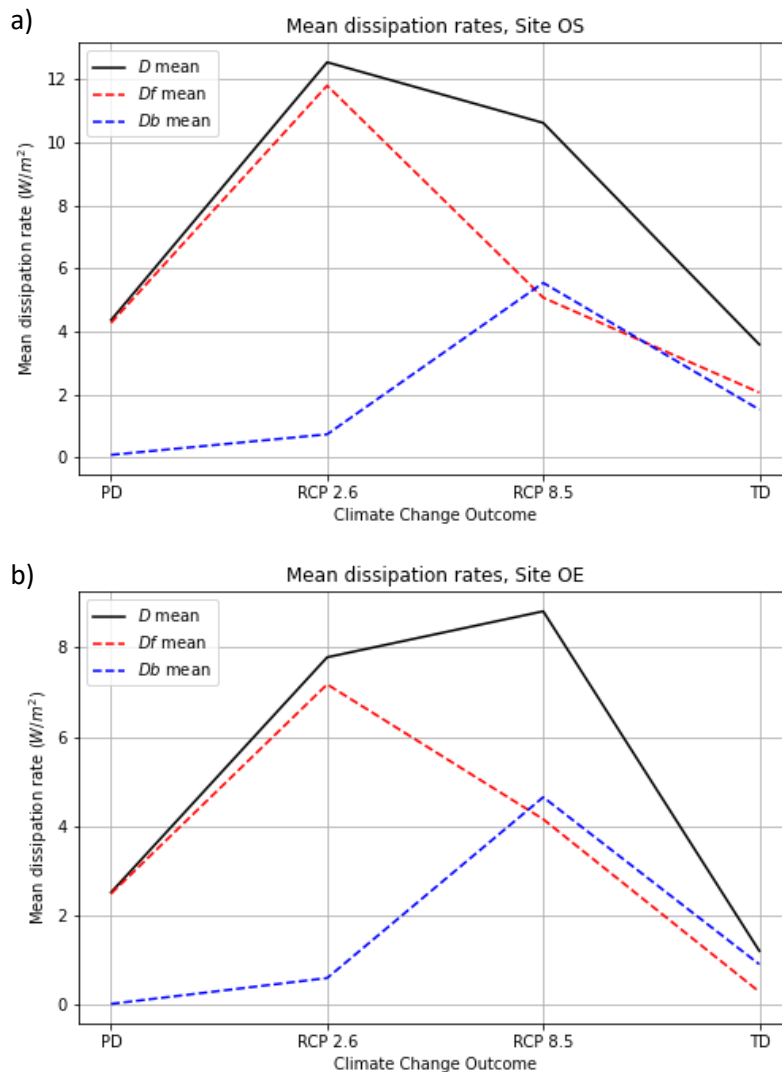
Figure 5: Maximum wave energy dissipation (blue) and dissipation due to bed friction (red) for across the x and time domains, for Site OS under a) RCP 2.6, b)

RCP 8.5 and c) TD climate change outcomes. for site OE under d) RCP 2.6, e) RCP 8.5 and f) TD climate change outcomes. Mean wave energy dissipations are

provided numerically for each plot. Note Y axis are unique for each study site to highlight relative differences in dissipation under variable climate change

outcomes.

278   Under present-day conditions, bed friction is dominant, contributing 98% and 99% of total wave

279   energy dissipation (Figures 5 and 6). Comparing RCP 2.6 to RCP 8.5, the OS site decreased frictional

280   dissipation by 57% and at site OE this was 42% (Figure 5 and Figure 6). In this case, dissipation by

281   wave breaking increased by an average of 659% for both sites. This results in a shift in the dominant

282   form of wave energy dissipation (Figure 6). Comparing RCP2.6 to the TD scenario, mean frictional

283   dissipation (D_f) decreases by 82.5% at site OS and 95.8% at site OE while wave breaking remains

284   marginally greater by 0.1% (OS) and 1.5% (OE) in the TD scenario. Despite this, mean total wave

285   energy dissipation (the sum of frictional and wave breaking dissipation rates) decreases by 71.4%

286   (OS) and 84.4% (OE).

a)

b)

287

288   *Figure 6: Mean total dissipation (D mean) for OS (a) and OE (b) study sites and mean dissipation by*

289   *bed friction (Df mean) and wave breaking (Db mean) for each climate change scenario (see Table 3).*

290   We calculated wave overtopping for both sites under present day conditions and three climate

291   change scenarios considering both mean and storm wave conditions (Table 2). For mean wave

292   conditions, wave overtopping in the present-day model was near zero (0 and 0.1 m at site OS and

293   OE, respectively). Wave overtopping increase for all forecast climate change scenarios (Figure 6). We

294   calculated overtopping of 0.4 m at site OS and 0.1 m at site OE for RCP 2.6 with larger increases to

295   0.4 m (OS) and 0.7 m (OE) for RCP8.5. The high emissions scenario (TD) had the highest overtopping

296   of 2.1 m (OS) and 2.0 m (OE).

297   Storm wave conditions increased overtopping compared to mean wave heights in all cases (Figure 7;

298   Table 2). Under present-day conditions, wave overtopping was greater than for mean wave

299   conditions at 1.25 and 0.5 m for site OS and site OE respectively. Under forecast climate change

300   scenarios, storm waves did not significantly impact overtopping under RCP2.6 compared to present

301   day conditions despite an increase in wave height of 3.5 m. Overtopping under RCP8.5 was 2.1 m at

302   site OS and 1.4 m at site OE which increased significantly to 3.5 m and 3.9 m in pessimistic TD

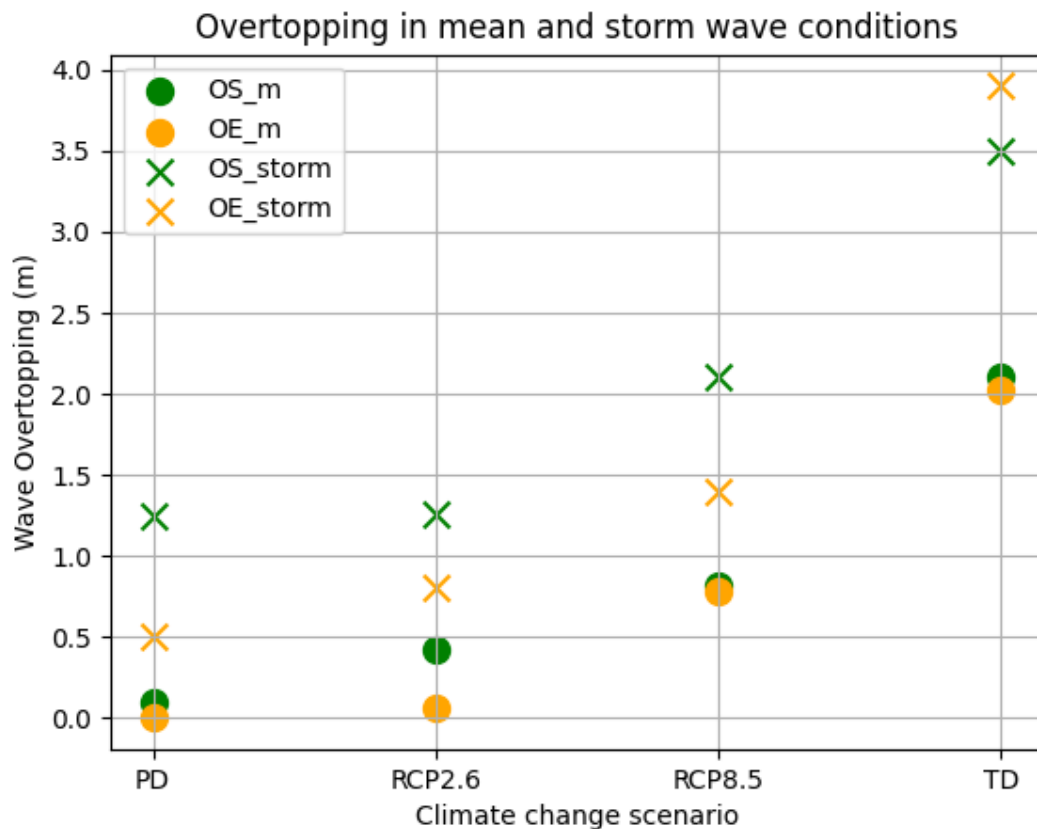303   models at each site respectively.

Figure 7: Wave overtopping at both sites under mean (OS_m and OE_m) and storm (OS_storm and OE_storm).

4. Discussion

4.1 Benefits of high-resolution LiDAR-derived bathymetries in numerical wave models

Our models of wave transformation over LiDAR-derived bathymetries focus on the influence of SaG morphology on wave energy dissipation and overtopping. Under mean wave conditions we calculated average dissipation rates across the entire forereef profile of 3.61 W/m^2 at site OS and 2.52 W/m^2 at site OE for offshore wave heights of 1.3 m and 1.2 m respectively. This calculation is made across the entire reef profile representing 862 m and 770 m respectively (Figure 2b, c). Field measurements of wave energy dissipation conducted at OTR were taken at the same site as OE presented in this study (Figure 2c) (Duce et al. 2022). We determined a mean dissipation rate of 10.6 W/m^2 across 60 m between the two instruments, almost entirely due to bed friction (Figure 4 d).

317   Duce et al. (2022) recorded mean dissipation rates of 20 W/m² with wave heights of $H_s = 0.78$ m and

318    $T_p = 5$ seconds. Differences in the recoded and modelled data at this site may be attributed to the

319   incident wave direction (N-NE during the deployment period) which was not completely aligned with

320   SaG as modelled here. These results compare with data obtained on a fringing reef in Ipan (Guam)

321   which also featured SaG on the forereef (Péquignet et al., 2011). Between two sensors placed 55 m

322   apart inside a 5 m deep groove, the dissipation rate was 25 W/m² for offshore wave heights of 1-2 m

323   (Péquignet et al., 2011). Monismith et al. (2015) identified comparable dissipation rates of 25 W/m²

324   on a forereef in Palmyra (Kiribati) between instruments 50 m apart for incident wave heights of 1 m.

325   Monismith et al. (2013) determined rates of 22 W/m² across a forereef at Mo'orea (French

326   Polynesia) with instruments located 50 m apart and wave heights of 0.3 to 0.5 m. Dissipation rates

327   for each of these studies are assumed to be due to bed friction with constant dissipation between

328   the instruments. Our results indicate that the dissipation rate across the forereef is heterogenous

329   and controlled by the bed morphology (e.g. Figure 5 a). The use of real bathymetries in modelling

330   efforts can elucidate the heterogeneity of dissipation rates on forereefs.

331   Using a real bathymetry, our study demonstrates the influence of groove sinuosity on wave energy

332   dissipation by breaking. Our results show that shore-normal waves interact with spur walls that do

333   not perfectly align with incoming swells. Indeed in our study, the mean groove heading was used to

334   align the bathymetric grids to the oncoming waves (Figure 2b), consistent with field observations

335   (Duce et al., 2020; Munk and Sargent, 1948). Despite this, variation in headings between grooves

336   and the sinuosity of individual grooves produces steep irregularities in the forereef slope that have a

337   large impact on the oncoming waves, playing a significant role on both dissipation by wave breaking

338   and bed friction. The straight and shore normal SaG identified in this analysis (mean sinuosity of

339   S=0.99, where 1 is a perfectly straight groove) (Table 4) are representative of groove sinuosity across

340   the southern Great Barrier Reef. For example, observations of 12,102 grooves in the GBR and South

341   Pacific show a mean groove sinuosity of S = 0.98 (Duce, 2017). Despite remarkable regional

342   consistency in groove morphology, we observed that even small deviations from perfect shore-

343   normal grooves are significant to wave transformation on the forereef. A more sensitive measure for

344   groove sinuosity may allow for a better understanding of forereef hydrodynamics. Further

345   investigation into SaG sinuosity effects should consider the natural sinuosity of SaG derived from

346   high resolution digital elevation models to account for these effects.

4.2 Effects of SaG from different morphological classes on wave energy dissipation

348   The most wave exposed site (southern site, OS) has the highest average dissipation rates of 71.5%

349   over 300 m SaG zone due to bed friction (Figure 4a). The long (mean length of 187.12 m) and deep

350   (mean depth of 1.95 m) exposed to wave energy (EWE) grooves at this exposed site may explain how

351   this high average dissipation rate occurred (Table 1). The length of EWE SaG creates surfaces of high

352   frictional drag that extend the zone of frictional dissipation and contribute to high average

353   dissipation rates (Figures 4a and 5). Shore normal currents occurring in the long and deep grooves

354   have also been observed and facilitate high rates of dissipation (Rogers et al., 2013). We

355   demonstrate under present-day conditions that bed frictional dissipation is dominant in dissipating

356   wave energy before breaking occurs at the reef crest (Figure 4a and c). Bed frictional dissipation

357   represents 98.0% and 98.9% of total dissipation at site OS and OE respectively (Figure 4a and c). This

358   is consistent with field research conducted at OTR (Duce et al., 2022) and in other high-energy

359   settings (Lowe et al., 2005; Monismith et al., 2015; Rogers et al., 2017). For example, under mean

360   wave conditions at Palmyra (Kiribati), a high bed friction coefficient (f_w =1.8) facilitated greater wave

361   energy dissipation due to bed friction than from wave breaking (Monismith et al., 2015), which is

362   consistent with field observations in Kaneohe Bay, Oahu, Hawaii (Lowe et al., 2005). Our results

363   suggest that the modes of wave energy dissipation (frictional or breaking) are not only influenced by

364   the wave conditions but also by the heterogenous morphology of the forereef slopes.

365   SaG morphology and consequently the morphological classes of Duce et al., (2016) can provide

366   further explanations to the mode of wave energy dissipation (Table 1). Where grooves are shorter,

367   they play a critical role in creating steep bathymetric gradients that induce wave breaking (Figures 4

368   and 8). This differs from previous SaG research (Acevedo-Ramirez et al., 2021) that showed wave

369   breaking being induced by the reef crest. Semi-exposed SaGs (represented here by site OE) are

370   typically shorter (mean length of 71.5 m) and shallower (mean depth of 1.38 m) than the most

371   exposed sites (site OS) and can include both exposed to wave energy (EWE) and deep and

372   disconnected (DaD) classes (Table 1). The seaward extent of the EWE grooves at semi-exposed

373   forereef sites (OE; Figure 4d) feature a steep bathymetric incline that produces the maximum wave

374   energy dissipation by wave breaking rate observed across all present-day models (1824.7 W/m^2,

375   Figure 5). As such, long spurs can facilitate frictional dissipation and short grooves can induce wave

376   breaking by introducing steep bathymetric inclines within the breaker zone of incident waves.
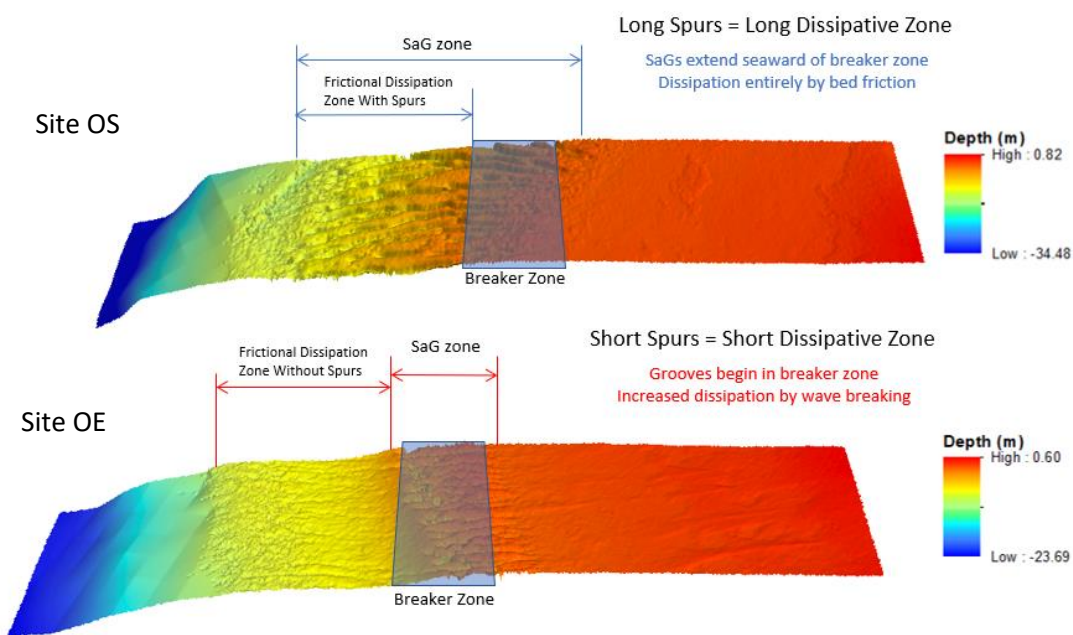

378   *Figure 8: A comparison between exposed and semi-exposed bathymetric profiles (site OS and site OE)*

379   *demonstrate the influence of the length of the SaG zone.*

380   The peak in wave energy dissipation at the shoreward of exposed to wave energy (EWE) grooves

381   highlights the complex interaction between forereef morphological evolution and wave energy

382   (Figure 4e). The seaward extent of EWE grooves is at a depth of 3.5 m, coincident with the mean

383   model wave height breaker depth for waves of 1.3 – 4.3 m (Figure 4, Table 2). As wave breaking

384   imposes forces on the structure of the reef (Massel & Gourlay, 2000; Storlazzi et al., 2005) the

385   results presented here suggest that incident waves could be capable of modifying the EWE grooves

386   in this zone, which is consistent with C14 and U-Th ages of SaG formations on the eastern forereef of

387   OTR (Duce et al., 2020), suggesting an erosive origin for this grooves. Imposed climate change effects

388   further elucidate the influence of grooves. Deep and disconnected (DaD) grooves at site OE exist

389   below the typical wave base and have minimal interaction with present day wave energy. Supporting

390   the previous findings that DaD grooves may be relict features, formed at an early stage during the

391   Holocene transgression (Duce et al., 2016).

4.3   The impact of climate change on wave energy dissipation over SaG

393   Forecasted environmental changes decrease mean wave energy dissipation (Figure 5) which is

394   consistent with other approaches (e.g., Quataert et al., 2015; Sheppard et al., 2005). In the

395   simulations presented here, dissipation remains high between RCP 2.6 and RCP 8.5 as reduced

396   dissipation by bed friction is balanced by an increase in dissipation by wave breaking (Figures 5 and

397   6). The difference between dissipation by bed friction and dissipation by wave breaking is the

398   greatest at both sites for RCP 8.5, where water depth is still sufficient for wave breaking, yet the

399   degradation of the reef reduces frictional effects (see Figure 9). A reliance on wave breaking

400   dissipation is consistent with observations from high energy reefs of low structural complexity

401   (Harris et al., 2018). Finally, dissipation is lowest where SLR is greatest (TD scenario) due to wave

402   passing over the reef without breaking (Figure 9). Although the role of SLR is thought to be

403   secondary in contributing to these changes (Harris et al., 2018), our models suggest that the

404   combined impact of SLR and loss of structural complexity will lead to lowest dissipation rates

405   (Figures 5 and 9) and highest wave overtopping (Figures 6 and 9) under future climate change

406   scenarios.

407   Sea-level rise (SLR) shifts the region of high energy dissipation toward the reef-crest (Figure 5b, c and

408   e, f). Bathymetric features that are submerged into the surf zone by rising relative sea level are likely

409   to influence wave breaking and frictional dissipation (Figure 5). This is evident in the shoreward

410   shifting dissipation zones (Figure 5) and as previous literature states (Massel and Gourlay, 2000) is a

411   threat to corals in this zone as wave breaking results in greater hydrodynamic forces on corals.

412   Corals previously protected from wave energy are likely to be species of lower mechanical strength

413   (Storlazzi et al., 2005). Under worse case scenarios (RCP 8.5) by the year 2100 it is likely that corals

414   of the same species may be weaker due to lower carbonate saturation in the water column (Eakin,

415   1996) or high frequency bleaching events (Hughes et al., 2017). Coral breakage is likely to occur here

416   and the corals that support a steep bathymetric incline with a high frictional coefficient responsible

417   for this peak in wave energy dissipation may have lower structural resilience by 2100 (Eakin, 1996).

418   High-energy SaG formations have been attributed to wave induced erosion, albeit at vastly different

419   timescales to sedimentary swash-zone features such as rip channels (Duce et al., 2020). It is possible

420   that climate change-driven increase in erosive forces promote further SaG development on

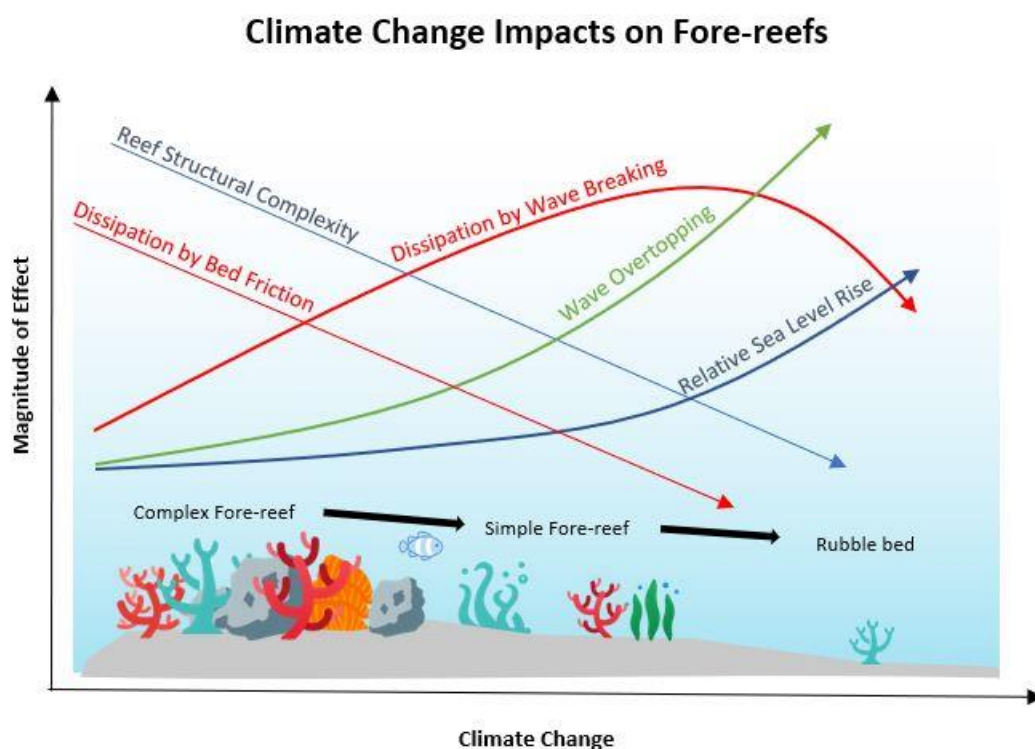421   forereefs, which contributes to the dissipation of wave energy.

422

423   *Figure 9: A conceptual diagram of changes to wave transformation on forereefs under increasing*

424   *climate change impacts. Climate driven inputs including loss of reef structural complexity and relative*

425   *sea-level rise are shown (blue). Dissipation rates (red) due to bed friction decreases, in response,*

426   *dissipation due to wave breaking increases until water depth exceeds breaker depths. Wave*

427   *overtopping (green) increases exponentially due to the combined effects of relative sea-level rise and*

428   *loss of reef structural complexity.*

4.3.2 Potential for wave overtopping with climate change

430   Wave overtopping exponentially increases with climate change due to the coupled effects of

431   decreased bed friction and loss of dissipation due to breaking (Figure 7). Compared to mean wave

432   conditions, the impact of storm waves results in increasingly greater overtopping when climate

433   projections are increased. (Figure 7). This effect is persistent despite the increased wave energy

434   dissipation at the semi-exposed forereef (site OE) under RCP 8.5 (Figure 4e). The primary control on

435   wave overtopping is sea-level rise, which incorporates eustatic and local sources. Future work should

436   include tidal effects, which would contribute an additional 1.5 m of water level at mean spring high

437   tide at OTR (Harris et al., 2015). The magnitude of wave overtopping observed in the TD scenario at

438   the exposed site (OS) of ~4 m is sufficient to entirely flood all backreef environments at OTR,

439   including the low-lying coral island. This magnitude of wave overtopping would have significant

440   impacts on coral reef islands and reef-lined shores(Fellowes et al. 2022; Storlazzi et al. 2015;

441   Talavera et al. 2021). For example, 3.7 m of wave run up combined with sea surface elevation above

442   a reef flat in Roi-Namur, Marshall Islands, was observed in flooding of inland area of the Island

443   (Cheriton et al., 2016). Research elsewhere demonstrated that wave overtopping on reef islands in

444   the year 2100 will be highly variable across due to variable reef vertical accretion and erosion rates

445   (Beetham and Kench, 2018; Kench et al., 2022), but also due to the vertical accretion of coral reef

446   islands (Kench et al., 2019, 2022; Masselink et al., 2020) which is controlled by sediment availability.

447   The combined influence of coral reef degradation and sea-level rise amplifies the occurrence of

448   wave overtopping, thereby exposing communities located in the downwind direction of coral reefs

449   to heightened risks of flooding (Harris et al., 2018; Quataert et al., 2015; Storlazzi et al., 2018).

450   Notably, a maximum overtopping of approximately 4 m was measured here when the significant

451   wave height reached 5.1 m. An examination of altimeter data reveals that within the 33-year data

452   span, wave heights have not surpassed this threshold (95th percentile wave height = 3.1 m) (Figure

453   S1, supplementary material). Consequently, further investigation is required to determine the

454   frequency of significant overtopping events at OTR.

455   5. Conclusion

456   This study combined numerical modelling and LiDAR-derived bathymetry to demonstrate the

457   importance of forereef spur and groove (SaGs) morphologies in modifying wave energy. Results

458   indicate that high resolution digital elevation models (< 1 m) can provide morphometric data to

459   examine wave transformation on forereefs comparable to field studies. We show that groove

460   sinuosity plays a role in wave transformation and should be considered in future research on wave

461   dissipation on forereefs. This highlights the need for accurate bathymetries in future studies of

462   forereef wave energy dissipation, as idealized bathymetries used in previous studies, using

463   numerical or physical modelling, cannot provide results comparable to field studies.

464   We demonstrate that SaG morphological classes exhibit distinct dissipation characteristics, with

465   some showcasing higher frictional dissipation and others exhibiting greater breaking dissipation.

466   Notably, spur length emerges as a critical factor in enhancing dissipation by bed friction. Among the

467   SaG morphological classes, exposed to wave energy (EWE) grooves have demonstrated the most

468   substantial dissipation rates, while deep and disconnected (DaD) grooves contribute less to the

469   dissipation process, particularly evident under future climate change scenarios.

470   Projected climate change conditions may lead to a decrease in wave energy dissipation on forereefs.

471   Indeed, the climate change scenarios analysed demonstrated that changes in the mode of wave

472   energy dissipation will likely occur. The most notable result was a decrease in dissipation by bed

473   friction from 100% of dissipation under present day conditions to 48% under RCP 8.5. This is

474   matched by a 52% increase in dissipation by wave breaking. Overall, we found a loss in wave energy

475   dissipation under future climate change scenarios leading to increased wave overtopping, with the

476   maximum overtopping occurring where dissipation was lowest. Forereef morphological adjustment

477   to increased dissipation by wave breaking may expose corals to erosion, a process which has been

478   linked to the formation of SaG. The results highlight the critical role of forereef morphology in wave

479   energy dissipation and the need for measures to promote coral growth to facilitate future

480   dissipation. The findings have implications for the modelling wave transformation over forereefs to

481   provide insight into the future habitability of exposed reef-lined coasts.

482   ## 6. Acknowledgements

491   ## Data Availability

492

493   XBeach version 1.22 (revision 4567) is used in this analysis and can be accessed through a Docker

494   image available at https://hub.docker.com/r/tristansalles/docker2xbeach. Python codes used to

495   interpret LiDAR derived bathymetry in XBeach can be found at https://github.com/Lachie-

496   Perris/XBeach_coral. Satellite altimeter derived wave heights for the southern GBR are provided in

497   csv format with python notebooks at https://github.com/Lachie-Perris/RADWAVE_OTI.

498   References

499   Acevedo-Ramirez, César A., W. Stephenson, S. Wakes, and I. Mariño-Tapia. 2021. "Wave

500   Transformation on a Fringing Reef System With Spur and Groove Structures." *Journal of*

501   *Geophysical Research: Oceans* 126(9):1–14. doi: 10.1029/2020JC016910.

502   Amores, Angel, Marta Marcos, Gonéri Le Cozannet, and Jochen Hinkel. 2022. "Coastal Flooding and

503   Mean Sea-Level Rise Allowances in Atoll Island." *Scientific Reports* 12(1):1–12. doi:

504   10.1038/s41598-022-05329-1.

505   Baldock, T. E., A. Golshani, D. P. Callaghan, M. I. Saunders, and P. J. Mumby. 2014. "Impact of Sea-

506   Level Rise and Coral Mortality on the Wave Dynamics and Wave Forces on Barrier Reefs."

507   *Marine Pollution Bulletin* 83(1):155–64. doi: 10.1016/j.marpolbul.2014.03.058.

508   Baldock, T. E., Behnam Shabani, David P. Callaghan, Zhifang Hu, and Peter J. Mumby. 2020. "Two-

509   Dimensional Modelling of Wave Dynamics and Wave Forces on Fringing Coral Reefs." *Coastal*

510   *Engineering* 155. doi: 10.1016/j.coastaleng.2019.103594.

511   Beaman, R. J. 2017. "High-Resolution Depth Model for the Great Barrier Reef - 30 M."

512   Beetham, E., and P. S. Kench. 2018. "Predicting Wave Overtopping Thresholds on Coral Reef-Island

513   Shorelines with Future Sea-Level Rise." *Nature Communications* 9(1). doi: 10.1038/s41467-018-

514   06550-1.

515   Buckley, Mark L., Ryan J. Lowe, Jeff E. Hansen, and Ap R. Van Dongeren. 2016. "Wave Setup over a

516   Fringing Reef with Large Bottom Roughness." *Journal of Physical Oceanography* 46(8):2317–33.

517   doi: 10.1175/JPO-D-15-0148.1.

518   Buddemeier, R. W., and S. V. Smith. 1988. "Coral Reef Growth in an Era of Rapidly Rising Sea Level:

519   Predictions and Suggestions for Long-Term Research." *Coral Reefs* 7(1):51–56. doi:

520   10.1007/BF00301982.

521   Castillo, Karl D., Justin B. Ries, Jack M. Weiss, and Fernando P. Lima. 2012. "Decline of Forereef

522   Corals in Response to Recent Warming Linked to History of Thermal Exposure." *Nature Climate*

523   *Change* 2(10):756–60. doi: 10.1038/nclimate1577.

524   Cheriton, Olivia M., Curt D. Storlazzi, and Kurt J. Rosenberger. 2016. "Observations of Wave

525   Transformation over a Fringing Coral Reef and the Importance of Low-Frequency Waves and

526   Offshore Water Levels to Runup, Overwash, and Coastal Flooding." *Journal of Geophysical*

527   *Research: Oceans* 121(9):6762–78. doi: 10.1002/2016JC012132.Received.

528   De'Ath, Glenn, Katharina E. Fabricius, Hugh Sweatman, and Marji Puotinen. 2012. "The 27-Year

529   Decline of Coral Cover on the Great Barrier Reef and Its Causes." *Proceedings of the National*

530   *Academy of Sciences of the United States of America* 109(44):17995–99. doi:

531   10.1073/pnas.1208909109.

532   Dechnik, Belinda, Jody M. Webster, Peter J. Davies, Juan-carlos Braga, and Paula J. Reimer. 2015.

533   "Holocene ' Turn-on ' and Evolution of the Southern Great Barrier Reef : Revisiting Reef Cores

534   from the Capricorn Bunker Group." *Marine Geology* 363:174–90. doi:

535   10.1016/j.margeo.2015.02.014.

536   Duce, Stephanie. 2017. "The Form, Function and Evolution of Coral Reef Spurs and Grooves."

537   University of Sydney.

538   Duce, Stephanie, Belinda Dechnik, Jody M. Webster, Quan Hua, James Sadler, Gregory E. Webb, Luke

539   Nothdurft, Marcos Salas-Saavedra, and Ana Vila-Concejo. 2020. "Mechanisms of Spur and

540   Groove Development and Implications for Reef Platform Evolution." *Quaternary Science*

541   *Reviews* 231. doi: 10.1016/j.quascirev.2019.106155.

542   Duce, Stephanie, A. Vila-Concejo, S. M. Hamylton, J. M. Webster, E. Bruce, and R. J. Beaman. 2016.

543   "A Morphometric Assessment and Classification of Coral Reef Spur and Groove Morphology."

544   *Geomorphology* 265:68–83. doi: 10.1016/j.geomorph.2016.04.018.

545   Duce, Stephanie, A. Vila-Concejo, Sarah Hamylton, Eleanor Bruce, and Jody M. Webster. 2014. "Spur

546   and Groove Distribution, Morphology and Relationship to Relative Wave Exposure, Southern

547   Great Barrier Reef, Australia." *Journal of Coastal Research* 70:115–20. doi: 10.2112/si70-020.1.

548   Duce, Stephanie, A. Vila-Concejo, R. J. Mccarroll, B. Yiu, L. A. Perris, and J. M. Webster. 2022. "Field

549   Measurements from Contrasting Reefs Show Spurs and Grooves Can Dissipate More Wave

550   Energy than the Reef Crest." *Earth and Space Science Open Archive ESSOAr* 413(August

551   2021):108365. doi: 10.1016/j.geomorph.2022.108365.

552   Eakin, C. M. 1996. "Where Have All the Carbonates Gone? A Model Comparison of Calcium

553   Carbonate Budgets before and after the 1982–1983 El Nino at Uva Island in the Eastern

554   Pacific." *Coral Reefs* 15(2):109–19. doi: 10.1007/bf01771900.

555   Fellowes, Thomas E., Ana Vila-Concejo, Shari L. Gallop, Mitchell D. Harley, and Andrew D. Short.

556   2022. "Wave Shadow Zones as a Primary Control of Storm Erosion and Recovery on Embayed

557   Beaches." *Geomorphology* 399:108072. doi: 10.1016/j.geomorph.2021.108072.

558   Ferrario, F., M. W. Beck, C. D. Storlazzi, F. Micheli, C. C. Shepard, and L. Airoldi. 2014. "The

559   Effectiveness of Coral Reefs for Coastal Hazard Risk Reduction and Adaptation." *Nature

560   Communications* 5:3794. doi: 10.1038/ncomms4794.

561   Harris, Daniel L., Hannah E. Power, Michael A. Kinsela, Jody M. Webster, and Ana Vila-Concejo. 2018.

562   "Variability of Depth-Limited Waves in Coral Reef Surf Zones." *Estuarine, Coastal and Shelf

563   Science* 211(December 2016):36–44. doi: 10.1016/j.ecss.2018.06.010.

564   Harris, Daniel L., Alessio Rovere, Elisa Casella, Hannah Power, Remy Canavesio, Antoine Collin,

565   Andrew Pomeroy, Jody M. Webster, and Valeriano Parravicini. 2018. "Coral Reef Structural

566   Complexity Provides Important Coastal Protection from Waves under Rising Sea Levels."

567   *Science Advances* 4(2). doi: 10.1126/sciadv.aao4350.

568   Harris, Daniel L., A. Vila-Concejo, J. M. Webster, and H. E. Power. 2015. "Spatial Variations in Wave

569   Transformation and Sediment Entrainment on a Coral Reef Sand Apron." *Marine Geology*

570   363:220–29. doi: 10.1016/j.margeo.2015.02.010.

571   Harris, Daniel L., Jody M. Webster, Ana Vila-concejo, Stephanie Duce, and Javier X. Leon. 2023.

572   "Geomorphology Defining Multi-Scale Surface Roughness of a Coral Reef Using a High-

573   Resolution LiDAR Digital Elevation Model." *Geomorphology* 439(September 2022):108852. doi:

574   10.1016/j.geomorph.2023.108852.

575   Hughes, Terry P., James T. Kerry, Mariana Álvarez-Noriega, Jorge G. Álvarez-Romero, Kristen D.

576   Anderson, Andrew H. Baird, Russell C. Babcock, Maria Beger, David R. Bellwood, Ray

577   Berkelmans, Tom C. Bridge, Ian R. Butler, Maria Byrne, Neal E. Cantin, Steeve Comeau, Sean R.

578   Connolly, Graeme S. Cumming, Steven J. Dalton, Guillermo Diaz-Pulido, C. Mark Eakin, Will F.

579   Figueira, James P. Gilmour, Hugo Harrison, Scott F. Heron, Andrew S. Hoey, Jean Paul A. Hobbs,

580   mia O. Hoogenboom, Emma V Kennedy, Chao Yang Kuo, Janice M. Lough, ryan J. Lowe, Gang

581   Liu, Malcolm T. McCulloch, Hamish A. Malcolm, michael J. McWilliam, John M. Pandolfi, rachel

582   J. Pears, morgan S. Pratchett, Verena Schoepf, Tristan Simpson, William J. Skirving, Brigitte

583   Sommer, Gergely Torda, David R. Wachenfeld, Bette L. Willis, and Shaun K. Wilson. 2017.

584   "Global Warming and Recurrent Mass Bleaching of Corals." *Nature* 543(7645):373–77. doi:

585   10.1038/nature21707.

586   Hughes, Terry P., James T. Kerry, Andrew H. Baird, Sean R. Connolly, Andreas Dietzel, C. Mark Eakin,

587   Scott F. Heron, Andrew S. Hoey, Mia O. Hoogenboom, Gang Liu, Michael J. McWilliam, Rachel J.

588   Pears, Morgan S. Pratchett, William J. Skirving, Jessica S. Stella, and Gergely Torda. 2018.

589   "Global Warming Transforms Coral Reef Assemblages." *Nature* 556(7702):492–96. doi:

590   10.1038/s41586-018-0041-2.

591   Jell, John S., and Gregory E. Webb. 2012. "Geology of Heron Island and Adjacent Reefs, Great Barrier

592   Reef, Australia." *Episodes* 35(1):110–19. doi: 10.18814/epiiugs/2012/v35i1/010.

593   Kench, Paul S., Edward P. Beetham, Tracey Turner, Kyle M. Morgan, Susan D. Owen, and Roger. F.

594   McLean. 2022. "Sustained Coral Reef Growth in the Critical Wave Dissipation Zone of a

595   Maldivian Atoll." *Communications Earth & Environment* 3(1):1–12. doi: 10.1038/s43247-021-

596   00338-w.

597   Kench, Paul S., Murray R. Ford, and Susan D. Owen. 2019. "Patterns of Island Change and Persistence

598   Offer Alternate Adaptation Pathways for Atoll Nations." *Nature Communications* 9(1). doi:

599   10.1038/s41467-018-02954-1.

600   Knutson, Thomas R., Joseph J. Sirutis, Ming Zhao, Robert E. Tuleya, Morris Bender, Gabriel A. Vecchi,

601   Gabriele Villarini, and Daniel Chavas. 2015. "Global Projections of Intense Tropical Cyclone

602   Activity for the Late Twenty-First Century from Dynamical Downscaling of CMIP5/RCP4.5

603   Scenarios." *Journal of Climate* 28(18):7203–24. doi: 10.1175/JCLI-D-15-0129.1.

604   Lashley, Christopher H., Dano Roelvink, Ap van Dongeren, Mark L. Buckley, and Ryan J. Lowe. 2018.

605   "Nonhydrostatic and Surfbeat Model Predictions of Extreme Wave Run-up in Fringing Reef

606   Environments." *Coastal Engineering* 137(October 2017):11–27. doi:

607   10.1016/j.coastaleng.2018.03.007.

608   Lowe, R. J., J. L. Falter, M. D. Bandet, G. Pawlak, M. J. Atkinson, S. G. Monismith, and J. R. Koseff.

609   2005. "Spectral Wave Dissipation over a Barrier Reef." *J. Geophys. Res* 110:4001. doi:

610   10.1029/2004JC002711.

611   Madin, Joshua S., and Sean R. Connolly. 2006. "Ecological Consequences of Major Hydrodynamic

612   Disturbances on Coral Reefs." *Nature* 444(7118):477–80. doi: 10.1038/nature05328.

613   Massel, S. R., and M. R. Gourlay. 2000. "On the Modelling of Wave Breaking and Set-up on Coral

614   Reefs." *Coastal Engineering* 39(1):1–27. doi: 10.1016/S0378-3839(99)00052-6.

615   Masselink, Gerd, Eddie Beetham, and Paul Kench. 2020. "Coral Reef Islands Can Accrete Vertically in

616   Response to Sea Level Rise." *Sci. Adv* 6(June):3656–66.

617   Meucci, Alberto, Ian R. Young, Mark Hemer, Ebru Kirezci, and Roshanka Ranasinghe. 2020.

618   "Projected 21st Century Changes in Extreme Wind-Wave Events." *Science Advances*

619   6(24):7295–7305. doi: 10.1126/sciadv.aaz7295.

620   Monismith, Stephen G., Liv M.M. Herdman, Soeren Ahmerkamp, and James L. Hench. 2013. "Wave

621   Transformation and Wave-Driven Flow across a Steep Coral Reef." *Journal of Physical*

622   *Oceanography* 43(7):1356–79. doi: 10.1175/JPO-D-12-0164.1.

623   Monismith, Stephen G., Liv M. M. Herdman, Soeren Ahmerkamp, and James L. Hench. 2013. "Wave

624   Transformation and Wave-Driven Flow across a Steep Coral Reef." *Journal of Physical*

625   *Oceanography* 43(7):1356–79. doi: 10.1175/JPO-D-12-0164.1.

626   Monismith, Stephen G., Justin S. Rogers, David Koweek, and Robert B. Dunbar. 2015. "Frictional

627   Wave Dissipation on a Remarkably Rough Reef." *Geophysical Research Letters* 42(10):4063–71.

628   doi: 10.1002/2015GL063804.

629   Montaggioni, Lucien F. 2005. "History of Indo-Pacific Coral Reef Systems since the Last Glaciation:

630   Development Patterns and Controlling Factors." *Earth-Science Reviews* 71(1–2):1–75. doi:

631   10.1016/j.earscirev.2005.01.002.

632   Munk, Walter H., and Martson C. Sargent. 1948. "Adjustment of Bikini Atoll to Ocean Waves."

633   *Transactions, American Geophysical Union* 29(6):855. doi: 10.1029/TR029i006p00855.

634   Osorio-Cano, Juan D., Juan C. Alcérreca-Huerta, Andrés F. Osorio, and Hocine Oumeraci. 2018. "CFD

635   Modelling of Wave Damping over a Fringing Reef in the Colombian Caribbean." *Coral Reefs*

636   37(4):1093–1108. doi: 10.1007/s00338-018-1736-4.

637   Pepper, A., and M. L. Puotinen. 2009. "Gremo: A GIS-Based Generic Model for Estimating Relative

638   Wave Exposure." *18th World IMACS Congress and MODSIM 2009 - International Congress on*

639   *Modelling and Simulation: Interfacing Modelling and Simulation with Mathematical and*

640   *Computational Sciences, Proceedings* 1964–70.

641   Péquignet, A. C., J. M. Becker, M. A. Merrifield, and S. J. Boc. 2011. "The Dissipation of Wind Wave

642   Energy across a Fringing Reef at Ipan, Guam." *Coral Reefs* 30(SUPPL. 1):71–82. doi:

643   10.1007/s00338-011-0719-5.

644   Péquignet, Anne-Christine N., Janet M. Becker, and Mark A. Merrifield. 2014. "Energy Transfer

645   between Wind Waves and Low-Frequency Oscillations on a Fringing Reef, Ipan, Guam." *Journal

646   of Geophysical Research: Oceans* 119(10):6709–24. doi: 10.1002/2014JC010179.

647   Perry, Chris T., Lorenzo Alvarez-Filip, Nicholas A. J. Graham, Peter J. Mumby, Shaun K. Wilson, Paul S.

648   Kench, Derek P. Manzello, Kyle M. Morgan, Aimee B. A. Slangen, Damian P. Thomson, Fraser

649   Januchowski-Hartley, Scott G. Smithers, Robert S. Steneck, Renee Carlton, Evan N. Edinger, Ian

650   C. Enochs, Nuria Estrada-Saldívar, Michael D. E. Haywood, Graham Kolodziej, Gary N. Murphy,

651   Esmeralda Pérez-Cervantes, Adam Suchley, Lauren Valentino, Robert Boenish, Margaret

652   Wilson, and Chancey MacDonald. 2018. "Loss of Coral Reef Growth Capacity to Track Future

653   Increases in Sea Level." *Nature* 558(7710):396–400. doi: 10.1038/s41586-018-0194-z.

654   Quataert, Ellen, Curt Storlazzi, Ap van Dongeren, and Robert McCall. 2020. "The Importance of

655   Explicitly Modelling Sea-Swell Waves for Runup on Reef-Lined Coasts." *Coastal Engineering*

656   160(April):103704. doi: 10.1016/j.coastaleng.2020.103704.

657   Quataert, Ellen, Curt Storlazzi, Arnold Van Rooijen, Olivia Cheriton, and Ap Van Dongeren. 2015a.

658   "The Influence of Coral Reefs and Climate Change on Wave-Driven Flooding of Tropical

659   Coastlines." *Geophysical Research Letters* 42(15):6407–15. doi: 10.1002/2015GL064861.

660   Quataert, Ellen, Curt Storlazzi, Arnold Van Rooijen, Olivia Cheriton, and Ap Van Dongeren. 2015b.

661   "The Influence of Coral Reefs and Climate Change on Wave-Driven Flooding of Tropical

662   Coastlines." *Geophysical Research Letters* 42(15):6407–15. doi: 10.1002/2015GL064861.

663   Reguero, Borja G., Iñigo J. Losada, and Fernando J. Méndez. 2019. "A Recent Increase in Global Wave

664   Power as a Consequence of Oceanic Warming." *Nature Communications* 10(1):1–14. doi:

665   10.1038/s41467-018-08066-0.

666   Roelvink, Dano, A. Reniers, Ap van Dongeren, J. S. M. van Thiel de Vries, J. Lescinski, and R. T. McCall.

667   2015. *XBeach Model Description and Manual*.

668   Rogers, Justin S., Stephen G. Monismith, Falk Feddersen, and Curt D. Storlazzi. 2013.

669   "Hydrodynamics of Spur and Groove Formations on a Coral Reef." *Journal of Geophysical*

670   *Research: Oceans* 118(6):3059–73. doi: 10.1002/jgrc.20225.

671   Rogers, Justin S., Stephen G. Monismith, Oliver B. Fringer, David A. Koweek, and Robert B. Dunbar.

672   2017. "A Coupled Wave-Hydrodynamic Model of an Atoll with High Friction: Mechanisms for

673   Flow, Connectivity, and Ecological Implications." *Ocean Modelling* 110. doi:

674   10.1016/j.ocemod.2016.12.012.

675   Rogers, Justin S., Stephen G. Monismith, David A. Koweek, and Robert B. Dunbar. 2016. "Wave

676   Dynamics of a Pacific Atoll with High Frictional Effects." *Journal of Geophysical Research:*

677   *Oceans* 121(1):350–67. doi: 10.1002/2015JC011170.

678   Sanborn, Kelsey L., Jody M. Webster, Gregory E. Webb, Juan Carlos Braga, Marc Humblet, Luke

679   Nothdurft, Madhavi A. Patterson, Belinda Dechnik, Susan Warner, Trevor Graham, Richard J.

680   Murphy, Yusuke Yokoyama, Stephen P. Obrochta, Jian xin Zhao, and Marcos Salas-Saavedra.

681   2020. "A New Model of Holocene Reef Initiation and Growth in Response to Sea-Level Rise on

682   the Southern Great Barrier Reef." *Sedimentary Geology* 397:105556. doi:

683   10.1016/j.sedgeo.2019.105556.

684   Saunders, Megan I., Simon Albert, Chris M. Roelfsema, Javier X. Leon, Colin D. Woodroffe, Stuart R.

685   Phinn, and Peter J. Mumby. 2016. "Tectonic Subsidence Provides Insight into Possible Coral

686   Reef Futures under Rapid Sea-Level Rise." *Coral Reefs* 35(1):155–67. doi: 10.1007/s00338-015-

687   1365-0.

688   Sheppard, Charles. 1981. "The Groove and Spur Structures of Chagos Atolls and Their Coral

689   Zonation." *Estuarine, Coastal and Shelf Science* 12(5):549–60. doi: 10.1016/S0302-

690   3524(81)80081-3.

691   Sheppard, Charles, David J. Dixon, Michael Gourlay, Anne Sheppard, and Rolph Payet. 2005. "Coral

692   Mortality Increases Wave Energy Reaching Shores Protected by Reef Flats: Examples from the

693   Seychelles." *Estuarine, Coastal and Shelf Science* 64(2–3):223–34. doi:

694   10.1016/j.ecss.2005.02.016.

695   Shinn, Eugene. 1963. "Spur and Groove Formation on the Florida Reef Tract." *SEPM Journal of*

696   *Sedimentary Research* Vol. 33(2):291–303. doi: 10.1306/74d70e34-2b21-11d7-

697   8648000102c1865d.

698   Shukla, P. R., J. Skea, R. Slade, R. van Diemen, E. Haughey, J. Malley, M. Pathak, and J. Portugal

699   Pereira. 2019. *IPCC, 2019: Technical Summary*.

700   Shukla, P. R., J. Skea, R. Slade, R. van Diemen, E. Haughey, J. Malley, M. Pathak, and J. Portugal

701   Pereira. 2019. *IPCC, 2019: Technical Summary*.

702   da Silva, Renan F., Curt D. Storlazzi, Justin S. Rogers, Johan Reyns, and Robert McCall. 2020.

703   "Modelling Three-Dimensional Flow over Spur-and-Groove Morphology." *Coral Reefs*. doi:

704   10.1007/s00338-020-02011-8.

705   Smith, Courtney, Tristan Salles, and Ana Vila-Concejo. 2022. "Offshore Wave Climate of the Great

706   Barrier Reef." *In Review* (0123456789). doi: 10.1007/s00338-023-02377-5.

707   Smith, Courtney, Ana Vila-Concejo, and T. B. Salles. 2020. "RADWave: Python Code for Ocean

708   Surface Wave Analysis by Satellite Radar Altimeter." *Journal of Open Source Software* 1(5):46.

709   doi: https://doi.org/10.21105/joss.02083.

710   Smyth, C., and Alex A. Hay. 2002. "Wave Friction Factors in Nearshore Sands." *Journal of Physical*

711   *Oceanography* 32(12):3490–98. doi: 10.1175/1520-0485(2002)032<3490:WFFINS>2.0.CO;2.

712   Sous, Damien, Samantha Maticka, Samuel Meulé, and Frédéric Bouchette. 2022. "Bottom Drag

713   Coefficient on a Shallow Barrier Reef." *Geophysical Research Letters* 1–12. doi:

714   10.1029/2021gl097628.

715   Storlazzi, C. D., E. K. Brown, M. E. Field, K. Rodgers, and P. L. Jokiel. 2005. "A Model for Wave Control

716   on Coral Breakage and Species Distribution in the Hawaiian Islands." *Coral Reefs* 24(1):43–55.

717   doi: 10.1007/s00338-004-0430-x.

718   Storlazzi, Curt D., Edwin P. L. Elias, and Paul Berkowitz. 2015. "Many Atolls May Be Uninhabitable

719   Within Decades Due to Climate Change." *Scientific Reports* 5(1):1–9. doi: 10.1038/srep14546.

720   Talavera, Lara, Ana Vila-Concejo, Jody M. Webster, Courtney Smith, Stephanie Duce, Thomas E.

721   Fellowes, Tristan Salles, Daniel Harris, Jon Hill, Will Figueira, and Jörg Hacker. 2021.

722   "Morphodynamic Controls for Growth and Evolution of a Rubble Coral Island." *Remote Sensing*

723   13(8):1–23. doi: 10.3390/rs13081582.

724   Yao, Yu, Yicheng Liu, Long Chen, Zhengzhi Deng, and Changbo Jiang. 2020. "Study on the Wave-

725   Driven Current around the Surf Zone over Fringing Reefs." *Ocean Engineering* 198. doi:

726   10.1016/j.oceaneng.2020.106968.

727   Young, I. R. 1992. "The Determination of Spectral Parameters from Significant Wave Height and Peak

728   Period." *Ocean Engineering* 19(5):497–508. doi: 10.1016/0029-8018(92)90008-R.

729

1   **The influence of coral reef spur and groove morphology on wave energy dissipation and**

2   **wave overtopping under future climate change scenarios**

3

4   **Lachlan Perris[1,*], Tristan Salles [1], Thomas E Fellowes[1], Stephanie Duce[2], Jody Webster[1], Ana Vila-**

5   **Concejo[1]**

6   [1] Geocoastal Research Group and Marine Studies Institute, School of Geosciences, The University of
7   Sydney, NSW, 2006, Australia

8   [2] College of Science and Engineering, James Cook University, Bebegu Yumba Campus, Townsville,
9   Queensland 4811, Australia

10   * Corresponding Author, lachlan.perris@sydney.edu.au

11

12   Key Points:

13   •   Accurate bathymetries (<1 m) in forereef wave energy dissipation models highlight
14   previously overlooked features of the forereef, including spurs and grooves (SaG).
15   •   SaG influence forereef wave energy dissipation and this influence can be related to the
16   SaG morphology.
17   •   Future climate change projections modify dissipation rates by shifting the dominant
18   mode of dissipation (from bed friction to wave breaking) leading to an increase wave
19   overtopping on forereefs.

20

Abstract

22   Coral reefs protect coastlines from inundation and flooding, servicing over 200 million people

23   globally. Wave transformation has previously been studied on coral reef flats with limited focus on

24   forereef zones where wave transformation is greatest during high-energy conditions. This study

25   investigates the role of forereef spur and groove (SaG) morphology on wave energy dissipation and

26   overtopping on coral reefs. Using XBeach on LiDAR-derived bathymetry, we reproduced dissipation

27   rates comparable to SaG field studies under present-day conditions. Our results highlight the

28   benefits of accurate bathymetries in forereef wave energy dissipation models, as they incorporate

29   critical morphological features (e.g., groove sinuosity, irregular forereef slopes) that exert control

30   over mode of wave energy dissipation (frictional and breaking). We then investigated changes to

31   wave energy dissipation and wave overtopping based on IPCC AR5 low and high emission scenarios

32   (RCP2.6 and RCP8.5) and a total disaster scenario (TD) for the year 2100 considering changes to SaG

33   morphology, wave power and relative sea-level rise. For RCP2.6, an increase in wave heights of 0.8

34   m and an increase in water level of 0.3 m resulted in a two-fold increase in dissipation rates. For

35   RCP8.5 and TD, with no increase in incident wave height, dissipation rates were 29% and 395% lower

36   than RCP2.6. This resulted in increased overtopping at the reef crest by 1.8 m and 2.7 m for RCP8.5

37   and TD scenarios, respectively, when compared to RCP2.6. Decreased dissipation rates and

38   increased wave overtopping in forecasted climate conditions suggest the need for strategies to

39   promote coral growth to facilitate high dissipation rates in the future. The results from our novel

40   modelling approach have implications for the future habitability of exposed reef-lined coasts due to

41   increased exposure to coastal flooding and island inundation.

Plain language summary

43   Coral reefs are essential for protecting coastlines from floods and waves, benefiting over 200 million

44   people worldwide. We studied how waves change as they approach coral reefs, focusing on the

45   forereef zone where wave transformation is most significant during high-energy conditions. The

46   shape of the forereef, specifically the spur and groove (SaG) morphology, plays a crucial role in how

47   much wave energy is dissipated and how much water spills over the reef.

48   Using a digital representation of waves over accurate reef shapes (known at bathymetry), we

49   simulated wave dissipation rates comparable to real-world SaG studies. Our findings emphasize the

50   importance of accurate representations of forereef shapes in models to predict wave energy

51   dissipation, as they consider critical features such as SaG which affect how waves transform and lose

52   energy.

53   Next, we investigated how wave energy dissipation and overtopping might change under different

54   future climate scenarios. We considered low and high emission scenarios (RCP2.6 and RCP8.5) from

55   the IPCC AR5 report and a total disaster scenario (TD) for the year 2100, factoring in changes to

56   forereef elevation, wave power, and sea-level rise.

57   Under the low emission scenario (RCP2.6), with a slight increase in wave heights and water levels,

58   we observed a doubling of wave energy dissipation rates. However, under the high emission

59   scenario (RCP8.5) and the total disaster scenario (TD), dissipation rates decreased significantly

60   compared to RCP2.6, resulting in more water moving over the reef crest during storms. This suggests

61   that future climate conditions may lead to increased flooding and inundation on reef-lined coasts,

62   putting communities at risk.

63   In summary, our study highlights the benefits of using accurate reef shapes in simulating wave

64   energy dissipation on coral reefs. Accurate bathymetries can incorporate features such as spurs and

65   grooves of different shapes, which modify wave dissipation. Wave energy dissipation changes when

66   climate change projections are incorporated into the simulations leading to an increase in energy

67   passing over the forereef.

1. Introduction

68

69   Coral reefs provide many ecosystem services including coastal hazard protection from ocean waves,

70   with over 200 million people worldwide depending on the stability of this service (Ferrario et al.,

71   2014). Coral reefs are topographically complex structures which contribute to the frictional

72   dissipation of waves, however this has been studied in greater details on the reef crest and reef flat

73   (Ferrario et al., 2014; Monismith et al., 2015; Péquignet et al., 2014; Yao et al., 2020) than on the

74   high-energy environments of the forereef slope (Acevedo-Ramirez et al., 2021; Duce et al., 2014,

75   2016, 2022; Monismith et al., 2013; Sheppard, 1981). Yet, wave breaking on the forereef slope is the

76   dominant form of wave energy dissipation under high-energy conditions (Osorio-Cano et al. 2018)

77   suggesting that it is a critical region for coastal protection (Quataert et al. 2015a). High dissipation

78   rates on the forereef are controlled by forereef morphology such as spurs and grooves (SaG)

79   (Monismith et al., 2013; Osorio-Cano et al. 2018).

80   SaG are shore-normal elongate ridges (spur) and troughs (groove) on the forereef slopes of many

81   coral reefs (Duce et al., 2016). Their size, spacing and orientation are typically aligned with incident

82   waves and consequently the morphometric classification of SaG (Duce et al., 2016) reflects the

83   influence of waves in their formation (Table 1). High energy forereefs feature more defined SaG than

84   low-energy ones (Duce et al., 2016; Rogers et al., 2013). Recent research shows high-relief (up to 10

85   m) spurs in the Mexican Caribbean have a large influence over wave transformation, with dissipation

86   in the SaG zone contributing a 35% in wave energy flux. Wave energy flux on the forereef occurs

87   mostly in the sea-swell frequency band (> 0.04 Hz). While infragravity waves (0.004-0.04 Hz) are

88   important to wave transformation over reef flats and in lagoons (Cheriton et al. 2016), field

89   measurements of waves over SaG have shown negligible energy in the infragravity bands (Duce et al.

90   2022). A recent investigation into SaG morphology demonstrates that SaG are not optimised to

91   maximise wave energy dissipation, with their morphology dissipating energy while allowing energy

92   propagation (and water, nutrients, and oxygen) to facilitate coral growth in the lagoon (Johannsen et

93   al., in review). Further field investigations are required but have been limited by the difficulty of

94   accessing highly exposed and turbulent forereef slopes (Sheppard 1981; Sous et al. 2022).

95   SaG morphologies have been overlooked in both physical (e.g., Buckley et al., 2016) and numerical

96   models (e.g. Baldock et al., 2020; Monismith et al., 2013; Osorio-Cano et al., 2018) of forereef wave

97   attenuation. For instance, numerical models that include SaG morphologies typically use idealised

98   bathymetries (e.g. da Silva et al., 2020; Rogers et al., 2013) with simplified morphologies that

99   overlook the irregularity and diversity of SaG. Consequently, the impact of SaG morphologies (Table

100   1) on wave attenuation is poorly understood (Duce et al., 2022; Monismith et al., 2013; da Silva et

101   al., 2020).

102   Table 1: Morphological categorisation of SaG (Duce et al., 2016).

Deep and Disconnected (DaD)	Grooves are disconnected from the reef crest and appear in deeper water (>5.5m) with limited hydrodynamic energy
Exposed to wave energy (EWE)	This morphology is heavily governed by the wave climate. Grooves are oriented perpendicular to incoming wave crests.
Log and protected (LaP)	Grooves are longer (>50m) and wider than more exposed grooves
Short and protected (SaP)	These grooves are narrower and shorter than Class 3.

103

104   Studies have shown that forereef morphologies including SaG will be impacted by climate change

105   (Castillo et al., 2012; De'Ath et al., 2012; Hughes et al., 2018) likely resulting in reduced coastal

106   protection (Baldock et al., 2014; Ferrario et al., 2014; Quataert et al., 2015; Sheppard et al., 2005)

107   and increased wave overtopping (Amores et al. 2022; Beetham and Kench 2018). Most notably, a

108   loss of structural complexity (roughness) in forereefs will reduce bed friction impacting wave

109   attenuation (Baldock et al., 2014; Harris et al., 2018; Monismith et al., 2015; Rogers et al., 2016).

110   These impacts are exacerbated by relative sea-level rise, changes in regional wave power (Meucci et

111   al., 2020; Reguero et al., 2019) and modification and intensification of storm climates (Knutson et al.,

112   2015) which all modify wave transformation processes on forereefs.

113   The overall aim of this paper is to provide understanding of present day and forecasted wave

114   attenuation by SaG on coral reefs. Both of which are critical for coral reef management plans and

115   climate change adaptation strategies. To achieve this, we first identify the benefits of high-resolution

116   LiDAR-derived bathymetries in numerical wave models. Then we employ these models to determine

117   how SaG of different morphological class affect the dissipation of wave energy. Finally, we

118   investigate the effects of climate change on wave energy dissipation over SaG.

2. Methods

2.1 Study Site

One Tree Reef (OTR) (23°30'S, 152°06'E) is located 84 km offshore of the NE Australian mainland in

the Capricorn Bunker Group, in the southern Great Barrier Reef (GBR) (Figure 1a). OTR is a lagoonal

platform reef with semi-diurnal tides with a mean spring tidal range of 3 m. The entire forereef of

OTR features SaG (Duce et al., 2016). The mean significant offshore wave height, $H_{s,mean}$ of 1.7 m

(Smith et al., 2022) is typically generated from persistent SE trade winds that dominate the Coral Sea

for over 70% of the year (Jell and Webb, 2012). Consequently, the south-eastern forereef is the most

exposed to ocean swells (Figure 1b). We considered two study sites featuring SaGs of varying

morphological class (Table 1) on the eastern and southern side of OTR (henceforth labelled OE and
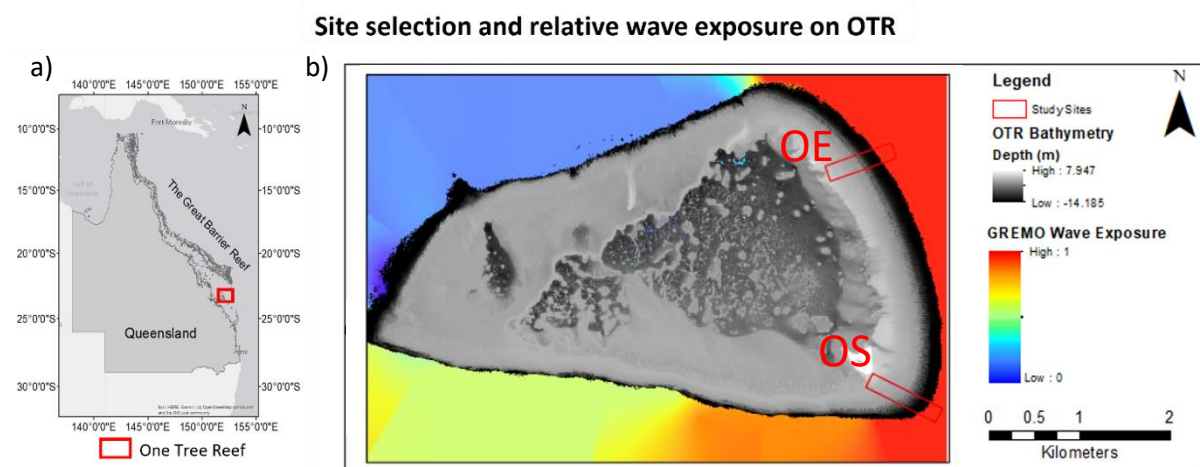
OS respectively) (Figure 1b, Table 1).

Figure 1: a) One Tree Reef (OTR) in the Southern Great Barrier Reef, and b) Study site locations for

OTR East (OE) and OTR South (OS) and relative wave exposure (Pepper and Puotinen 2009).

2.2 SaG morphometric analysis

We determined morphometric parameters for SAG in the two study sites including length, depth,

width, and others (Table 2) from analysis of LiDAR derived bathymetry and used them to classify the

SAG following the categorical framework of Duce et al. (2016) (Table 1).

137   Table 2: Morphometric parameters of SaG adapted from Duce et al. (2016).

Morphometric parameter	Method
Length (L)	Path distance along the groove (m)
Depth (D)	The vertical distance between the lowest point in the groove and the highest point on the neighbouring spur is calculated at four depths below sea level (-2, -4, -6, and -8 meters).
Width (W)	Groove width is measured as the horizontal distance between its walls at half the depth, along isobaths of -2, -4, -6 and -8 m.
Orientation (θ)	Azimuth of straight line between maximum onshore and offshore extents of groove
Sinuosity (S)	Ratio of straight-line distance (D) to path length (L) such that: $S = D/L$
Wavelength (γ_{sag})	The horizontal distance between the highest points of adjacent ridges, parallel to isobaths, measured at depths of -2, -4, -6, and -8 meters below mean sea level.

138

2.3. Wave transformation modelling (XBeach)

140   We used XBeach (Roelvink et al., 2015) in Surf Beat mode to understand hydrodynamics and wave

141   attenuation over SaG because it has been extensively validated on complex coral reef bathymetries

142   (Harris et al., 2018; Lashley et al., 2018; Quataert et al., 2015, 2020; da Silva et al., 2020).

2.3.1 Bathymetric Grids

144   We merged data from a 0.5 m resolution Airborne LiDAR survey (Harris et al., 2023) to a depth of 14

145   m, and a 30 m resolution bathymetry survey (Beaman, 2017) to a maximum depth of 20 m (Figure

146   2). This maximum depth was selected to capture all depth-limited wave breaking within the model

147   and was based on historical wave heights for OTR considering,

Eq. 1   7
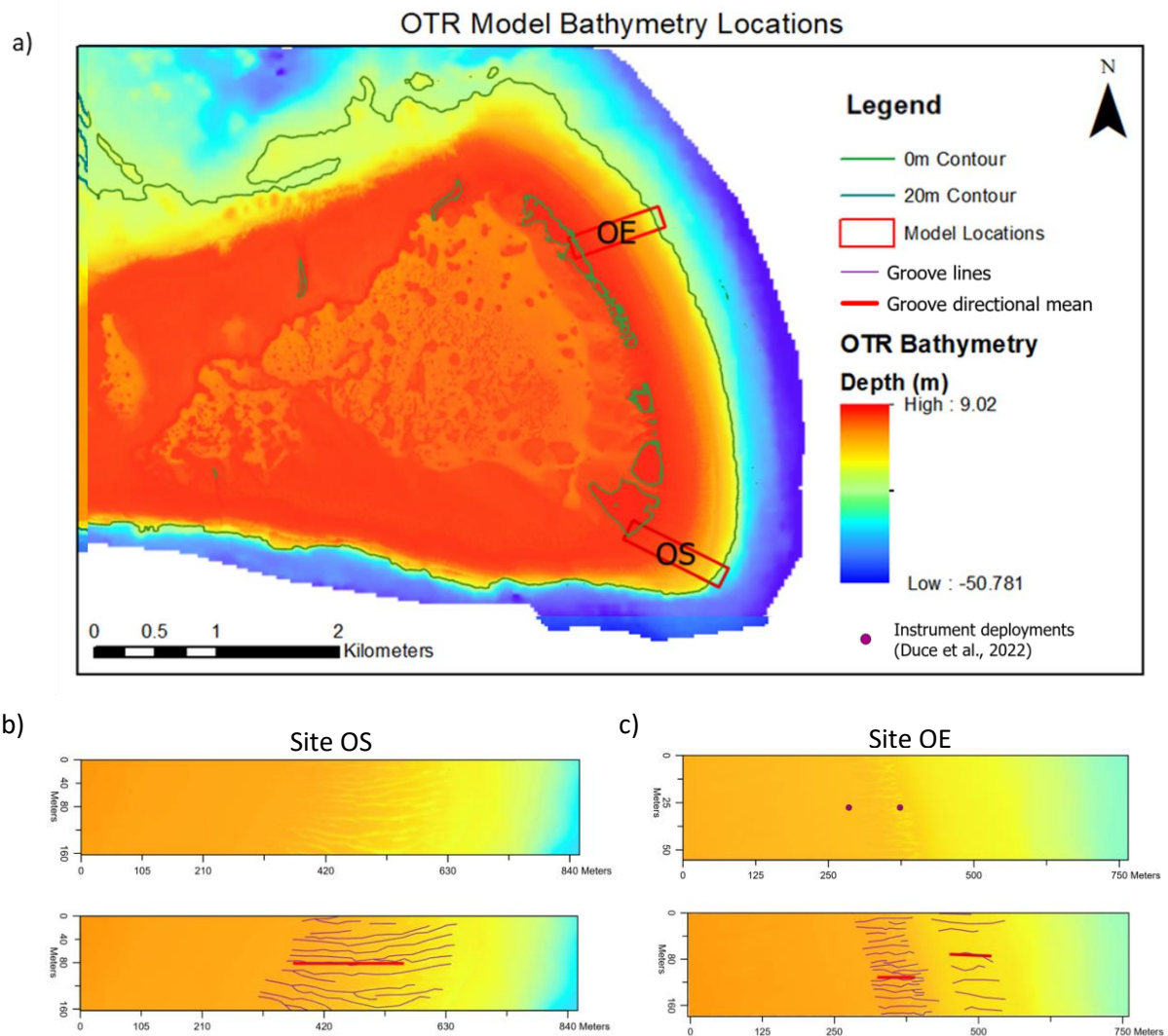
148
$$H_{max} = \gamma \cdot (h + \delta H_{rms})$$

149   where, γ is the breaker index, δH_{rms} is some fraction δ of the root mean square of the wave height.

150   The breaker index was held constant across the reef at $\gamma = 0.55$, reflecting the conservative

151   estimation ($\gamma = 0.55$) of (Duce et al., 2022) and within the ranges determined by Harris et al. (2018).

152

153   *Figure 2: a) The bathymetric grids used in wave models from two study sites on the eastern (OE) and*

154   *southern (OS) exposed forereefs of on One Tree Island. Grooves are shown in purple with the*

155   *directional mean of SaG shown in red.*

156   The outer boundaries of the bathymetric grids were oriented to align mean groove headings with

157   incident waves (Figure 2b and c), following field observations (Duce et al., 2014; Munk and Sargent,

158   1948; Shinn, 1963) and other wave transformation models constructed over SaG (Rogers et al., 2013;

159   da Silva et al., 2020) (Figure 2b). Offshore boundaries were set beyond the maximum breaker depth

160   for modelled wave heights (20 m: Eq. 1) and the onshore boundaries at present-day 0 m MSL

161   contour (Figure 2b, c). Consequently, grids for each site are of different length and width (Figure 2b).

162   ## 2.3.2 Climate change projections

163   We considered four climate change scenarios projected for the year 2100 including critical climate

164   impacts to wave energy dissipation on coral reefs: sea-level change, reef health and wave energy

165   conditions. The climate change scenarios are based on IPCC AR5 and include (1) the *present-day*

166   scenario considering no change to current environmental factors, (2) the *low* (RCP 2.6) and (3) *high*

167   (RCP8.5) emission scenarios from the AR5 IPCC report (Shukla et al., 2019), and (4) a *total disaster*

168   (TD) scenario included to represent a high carbon future.

169   *2.3.2.1 Changes to Sea Level*
170   We used IPCC AR5 sea-level rise (SLR) rate of 3 mm/yr (Shukla et al., 2019). Under the *low* and *high*

171   emission scenarios (RCP2.6 and RCP8.5) SLR is expected to reach up to 10-20 mm/yr. Subsequently,

172   we have included SLR of 0.43 m (RCP2.6) and 0.84 m (RCP8.5) for the year 2100 (Shukla et al., 2019).

173   Human stressors (e.g., infrastructure development and human-induced habitat degradation) are also

174   likely to contribute to increases in local SLR (Shukla et al., 2019). An additional 1 m of eustatic SLR

175   was included for our *total disaster* (TD) scenario to reflect significant changes to climate conditions

176   and non-climatic anthropogenic stressors (Shukla et al., 2019) (Table 3). The total sea-level increase

177   in each of the models (Table 3) was determined by the sum of eustatic and local sea-level changes,

178   and the vertical accretion and erosion of the reefs.

179   *2.3.2.2 Reef Morphological Changes*
180   Reef morphological changes have been simplified into three key characteristics, reef vertical

181   accretion, erosion, and structural complexity. A forecasted vertical accretion rate of 2 mm/yr was

182   used based on field measurements from coral reef cores from across the GBR (Dechnik et al., 2015;

183   Sanborn et al., 2020), Western Australia (Perry et al., 2018), Tahiti (Buddemeier and Smith, 1988),

184   the Maldives (Kench et al., 2022), Indo-Pacific averages compiled by Montaggioni (2005) and the

185   Solomon Islands (Saunders et al., 2016). Alternatively, erosion of forereefs can occur due to the

186   physical removal of coral and framework by storms and high wave energy (Madin and Connolly,

187   2006). This is most evident on degraded coral reefs where erosion has been observed at 6 mm/yr

188   (Eakin, 1996; Sheppard et al., 2005). We used a conservative estimate of 2.6 mm/yr (0.2 m by 2100)

189   of reef erosion for RCP 8.5 and a maximum of 6.4 mm/yr (0.5 m by 2100) of erosion under a TD

190   scenario, modelled as a uniform decrease in elevation over the simulated domain. The resulting sea

191   level was determined by combining projected rates of SLR with erosion and accretion values for each

192   scenario (Table 3).

193   To simulate a loss in forereef structural complexity, we altered the dimensionless wave friction

194   factor (f_w) to replicate changes to coral structural complexity. In our study, f_w were linearly

195   interpolated between $f_w = 0.9$ (healthy reef) to $f_w = 0.1$ (degraded or smoothed reef). For the *total*

196   *disaster* (TD) scenario, which represents a degraded reef and a shift to a carbonate sand substrate

197   we used $f_w = 0.01$ (Smyth and Hay, 2002) (Table 3).

2.3.3 Wave Input Parameters

199   Mean offshore wave conditions were determined by satellite altimeter observations over 30 years

200   (1985–2015) using RADWave (Smith et al., 2020) (Table 3). A small region (0.6° x 0.4°) representing

201   dense altimeter data tracks was identified on the eastern, exposed side of OTR (Figure S1). We

202   determined site-specific model input wave heights (H_{model}) by combining offshore wave conditions

203   with a relative wave exposure model, GREMO (GIS-based generic model for estimating relative wave

204   exposure; see Figure 1b) following Pepper and Puotinen (2009),

205    $$H_{model} = K_r \ H_{offshore} \qquad\qquad (1)$$

206   where, $H_{offshore}$ is the offshore wave height obtained from RADWave (Figure 1b and Figure S1) and

207   K_r is the relative exposure coefficient, normalised between 1 (most exposed) and 0 (least exposed).

208   Finally, altimeter wave heights were compared to measured waves at the northern forereef at OTR

209   (Duce et al., 2022).

210   2.3.4 Changes to wave climate

211   We increased offshore model wave heights ($H_{offshore}$) for future climate change scenarios (Table 3)

212   with wave periods (T_{model}) determined for a fully developed sea-state from the Joint North Sea Wave

213   Project (JONSWAP) spectrum (Young, 1992). Storm waves were calculated from the maximum wave

214   height observed in RADWave altimeter data. The final model wave heights were dependent on

215   forereef location and relative exposure to wave energy determined by Eq. 1.

216   *Table 3: Model input parameters are presented for three study sites, two wave conditions and four*

217   *forecasted climate outcomes for the year 2100. A total of 16 unique models were run.*

Site	Climate scenario	Wave Condition	$H_{offshore}$ (m)	Exposure Factor	H model (m)	T_{model} (s)	Friction factor	SLR (m)	Vertical Accretion (m)	Reef erosion (m)	Total change in MSL (m)
OS	Present day	Mean	1.34	0.985	1.3	5.74	0.9	0	0	0	0
	RCP 2.6		2.14				0.54	0.43	0.16	0	0.3
	RCP 8.5		2.14		2.1	7.26	0.1	0.84	0.1	0.2	0.99
	TD		2.14				0.01	1.84	0	0.5	2.34
	Present day	Storm	4.8		4.7	10.87	0.9	0	0	0	0
	RCP 2.6						0.54	0.43	0.16	0	0.3
	RCP 8.5		5.6		5.5	11.74	0.1	0.84	0.1	0.2	0.99
	TD						0.01	1.84	0	0.5	2.34
OE	Present day	Mean	1.34	0.9042	1.2	5.5	0.9	0	0	0	0
	RCP 2.6		2.14				0.54	0.43	0.16	0	0.3
	RCP 8.5		2.14		1.9	6.96	0.1	0.85	0.1	0.2	0.99
	TD		2.14				0.01	1.84	0	0.5	2.34
	Present day	Storm	4.8		4.3	10.42	0.9	0	0	0	0
	RCP 2.6		5.6				0.54	0.43	0.16	0	0.3
	RCP 8.5		5.6		5.1	11.25	0.1	0.84	0.1	0.2	0.99
	TD		5.6				0.01	1.84	0	0.5	2.34

218

219   2.3.5 XBeach model outputs

220   Each model was run for a total of 300 seconds, and we analysed the outputs of Xbeach for water

221   surface elevation (zs), total dissipation rate (D), and dissipation rate due to bed friction (D_f) to

222   obtain wave energy dissipation rates and wave overtopping. Total dissipation was used to compare

223   Xbeach results with field measurements and to determine dissipation by breaking (D_b) such that

224    $D_b = D - D_f$. As models are two-dimensional (x, y spatial domains) and evolve through time (t), we

225   calculated mean and peak dissipation rates across t and x domains for the entire bathymetric grid.

226   Mean dissipation rates were also taken between two points where hydrodynamic data sampled by

227   Duce et al. (2022). Wave overtopping was calculated as the difference between the initial water level

228   at the reef crest and the maximum water level at the reef crest during each model run.

3. Results

230   3.1 SaG morphometric analysis

231   SaG morphometrics were quantified for 123 grooves across the two study sites (Table 3). Grooves at

232   the southern site (OS) were on average 3 times longer, 1.4 times deeper and 1.3 times wider than

233   those at the eastern site (OE) (Table 3). Using the morphometric classification of Duce et al. (2016),

234   the exposed to wave energy (EWE) grooves were the most common across three of the four sites

235   (100 of 123 SaG) (Table 3). Deep and disconnected (DaD) grooves were present on the lower

236   forereef platform of site OE.

237   *Table 4: Morphometric parameters and classes of SaG at two study sites.*

	Mean SaG Morphometric Parameters					Quantity of SaG Classes by Site			
Site	Length (m)	Sinuosity	Orientation (Deg)	Depth (m)	Width (m)	DaD	EWE	LaP	SaP

| OS (south) | 187.12 | 0.99 | 116.73 | 1.95 | 4.02 | 0 | 40 | 0 | 0 |
| OE (east) | 63.18 | 0.99 | 71.5 | 1.38 | 3.12 | 23 | 60 | 0 | 0 |

238

3.2 Wave transformation over LiDAR derived bathymetry

240   The peak dissipation rates under present day conditions, taken as the maximum dissipation across

241   all axes (x, y, t), were 463.9 and 946.3 W/m^2 at sites OE and OS respectively (Figure 4). Wave energy

242   dissipation due to bed friction was dominant in present day scenarios over dissipation due to wave

243   breaking (Figure 4b and d). Between the two locations of field measurements conducted by Duce et

244   al., (2022) (Figure 2c) the mean dissipation rate was 10.6 W/m^2, the maximum dissipation rate of

245   463.9 W/m^2 occurred during this zone. Wave energy dissipation by bed friction contributed 78% of

246   energy at the site OE before waves reached the reef crest, 67% at site OS in the upper forereef

247   slope. The maximum wave energy dissipation due to wave breaking constituted 22%, and 32% of

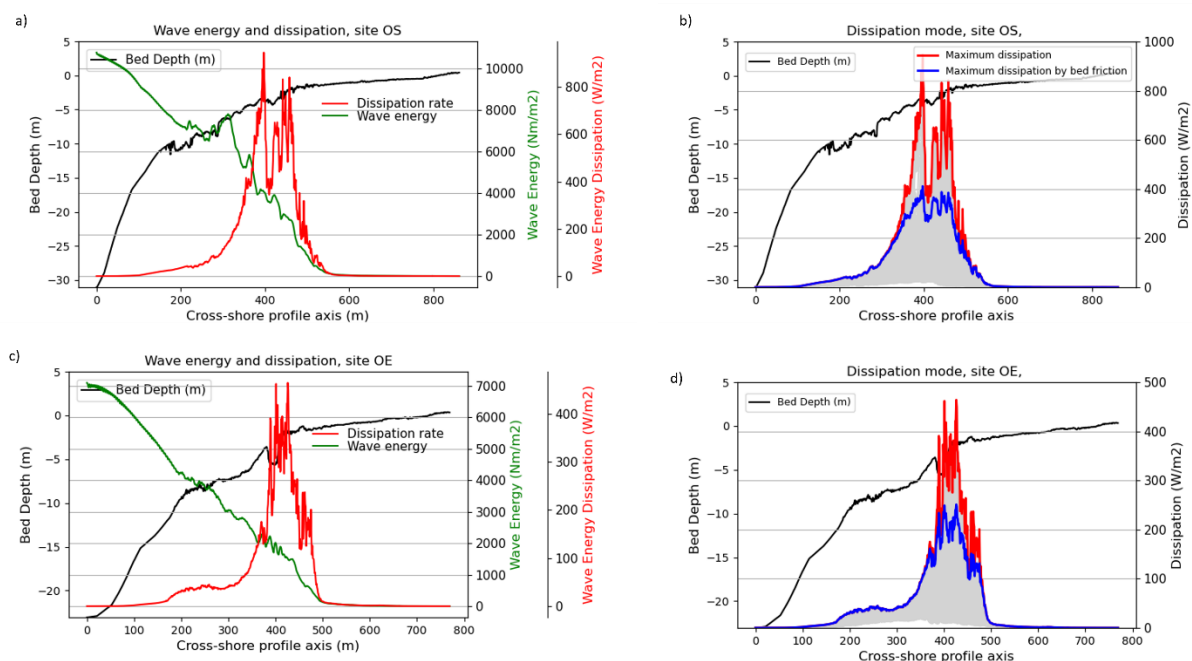248   total dissipation at site OE and OS respectively (Figure 4b, d).

249

250   *Figure 4: Wave energy (green) and maximum wave energy dissipation at site OS (a) and site OE (c).*

251   *Maximum dissipation and maximum dissipation by bed friction (blue) for site OS (b) and site OE (d).*

252   *Note different scale bars are used for each site.*

3.3 Wave transformation under future climate change projections

254   Wave transformation was found to vary greatly among models depending on climate change

255   scenario, SaG morphometrics, and wave exposure. The largest influence on wave energy dissipation

256   across the two sites was the reduction of the bed friction factor (f_w), increased water depth, and

257   increased wave height. Total wave energy dissipation and dissipation due to bed friction changed at

258   both sites for all future climate scenarios (Table 3).

259   Mean and peak dissipation rates were computed for each site across all three climate scenarios

260   (Table 3, Figure 5). When comparing dissipation rates from present day to RCP2.6 for the year 2100,

261   mean dissipation increased by 187% at site OS (4.4 to 12.5 W/m^2) and maximum dissipation

262   increased by 59.7% (946.3 to 1511.4 W/m^2) (Figure 5a and b). At site OE, mean dissipation rate

263   increased by 208.6% (2.5 to 7.8 W/m^2) and maximum dissipation increased by 217.7% (463.9 to

264   1473.4 W/m^2) (Figure 5d and e).

265   When comparing RCP2.6 to RCP8.5 we found a decrease in mean dissipation across site OS of 18.1%

266   (12.5 to 10.6 W/m^2) and an increased in the max dissipation rate of 23.2% (1511.4 to 1966.9 W/m^2).

267   Site OE retained at high mean dissipation rate from RCP2.6 to RCP8.5, increasing a further 11.7%

268   (7.78 to 8.81 W/m^2) and an increase of 19.3% to peak dissipation rate (1473.42 to 1824.70 W/m^2).

269   When comparing to RCP8.5, the TD scenario, mean dissipation rates decreased by 66.2% (10.61 to

270   3.58 W/m^2) at site OS and a decrease in peak dissipation of 31.8% (1966.89 to 1340.93 W/m^2)

271   (Figure 4b and c). At site OE, mean dissipation decreased by 86.2% (8.81 to 1.21 W/m^2) and peak

272   dissipation rate decreased by 75.4% (1824.7 to 448.24 W/m^2) (Figure 5e and f).
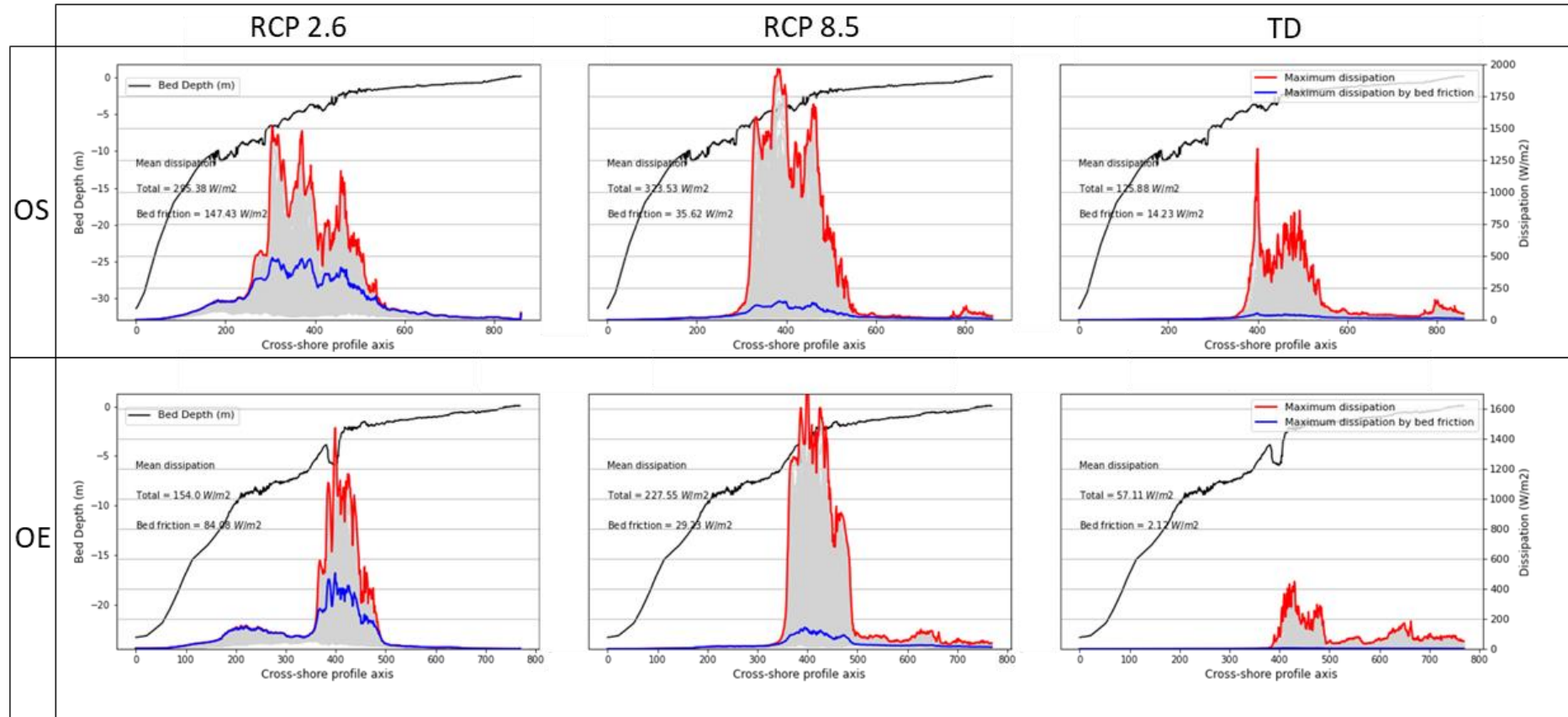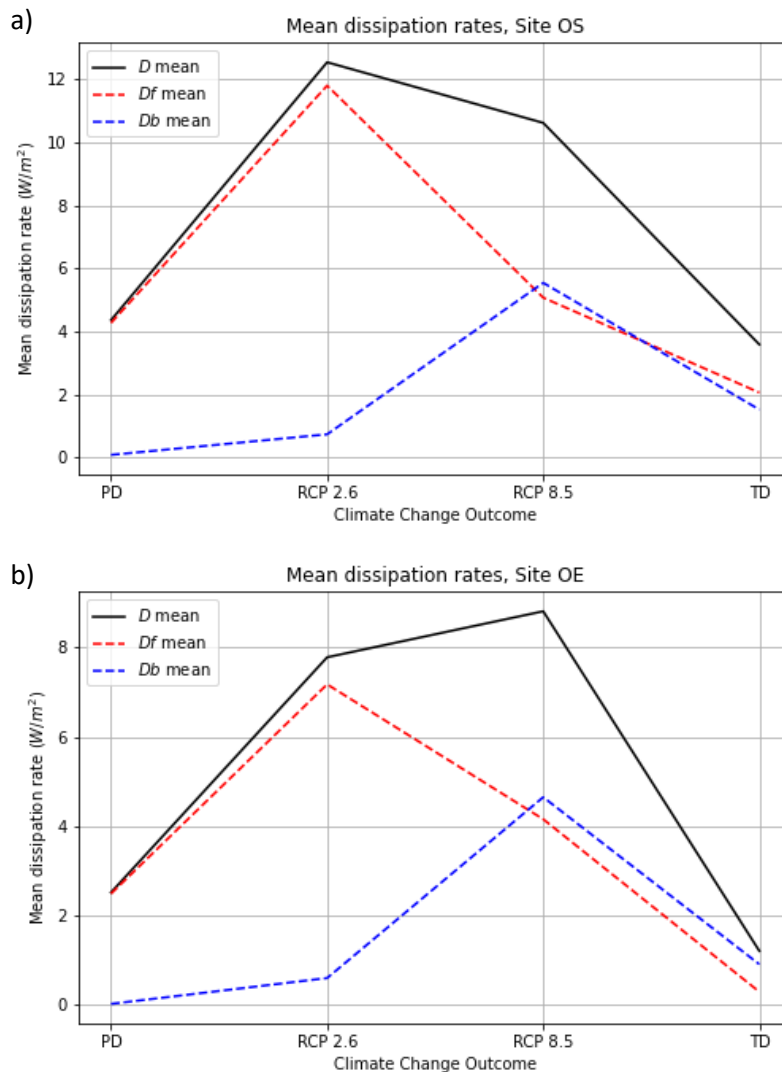
273

Figure 5: Maximum wave energy dissipation (blue) and dissipation due to bed friction (red) for across the x and time domains, for Site OS under a) RCP 2.6, b)

RCP 8.5 and c) TD climate change outcomes. for site OE under d) RCP 2.6, e) RCP 8.5 and f) TD climate change outcomes. Mean wave energy dissipations are

provided numerically for each plot. Note Y axis are unique for each study site to highlight relative differences in dissipation under variable climate change

outcomes.

278   Under present-day conditions, bed friction is dominant, contributing 98% and 99% of total wave

279   energy dissipation (Figures 5 and 6). Comparing RCP 2.6 to RCP 8.5, the OS site decreased frictional

280   dissipation by 57% and at site OE this was 42% (Figure 5 and Figure 6). In this case, dissipation by

281   wave breaking increased by an average of 659% for both sites. This results in a shift in the dominant

282   form of wave energy dissipation (Figure 6). Comparing RCP2.6 to the TD scenario, mean frictional

283   dissipation (D_f) decreases by 82.5% at site OS and 95.8% at site OE while wave breaking remains

284   marginally greater by 0.1% (OS) and 1.5% (OE) in the TD scenario. Despite this, mean total wave

285   energy dissipation (the sum of frictional and wave breaking dissipation rates) decreases by 71.4%

286   (OS) and 84.4% (OE).

a)

b)

287

288   *Figure 6: Mean total dissipation (D mean) for OS (a) and OE (b) study sites and mean dissipation by*

289   *bed friction (Df mean) and wave breaking (Db mean) for each climate change scenario (see Table 3).*

290   We calculated wave overtopping for both sites under present day conditions and three climate

291   change scenarios considering both mean and storm wave conditions (Table 2). For mean wave

292   conditions, wave overtopping in the present-day model was near zero (0 and 0.1 m at site OS and

293   OE, respectively). Wave overtopping increase for all forecast climate change scenarios (Figure 6). We

294   calculated overtopping of 0.4 m at site OS and 0.1 m at site OE for RCP 2.6 with larger increases to

295   0.4 m (OS) and 0.7 m (OE) for RCP8.5. The high emissions scenario (TD) had the highest overtopping

296   of 2.1 m (OS) and 2.0 m (OE).

297   Storm wave conditions increased overtopping compared to mean wave heights in all cases (Figure 7;

298   Table 2). Under present-day conditions, wave overtopping was greater than for mean wave

299   conditions at 1.25 and 0.5 m for site OS and site OE respectively. Under forecast climate change

300   scenarios, storm waves did not significantly impact overtopping under RCP2.6 compared to present

301   day conditions despite an increase in wave height of 3.5 m. Overtopping under RCP8.5 was 2.1 m at

302   site OS and 1.4 m at site OE which increased significantly to 3.5 m and 3.9 m in pessimistic TD

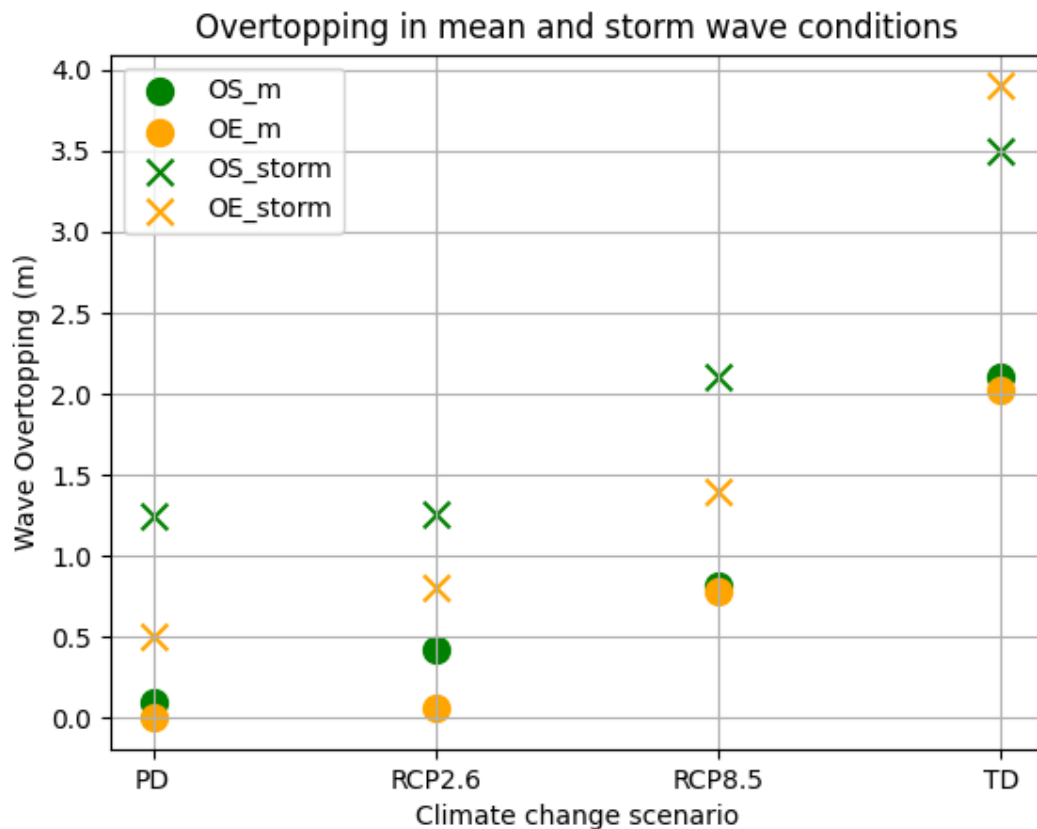303   models at each site respectively.

Figure 7: Wave overtopping at both sites under mean (OS_m and OE_m) and storm (OS_storm and OE_storm).

4. Discussion

4.1 Benefits of high-resolution LiDAR-derived bathymetries in numerical wave models

Our models of wave transformation over LiDAR-derived bathymetries focus on the influence of SaG

morphology on wave energy dissipation and overtopping. Under mean wave conditions we

calculated average dissipation rates across the entire forereef profile of 3.61 W/m^2 at site OS and

2.52 W/m^2 at site OE for offshore wave heights of 1.3 m and 1.2 m respectively. This calculation is

made across the entire reef profile representing 862 m and 770 m respectively (Figure 2b, c). Field

measurements of wave energy dissipation conducted at OTR were taken at the same site as OE

presented in this study (Figure 2c) (Duce et al. 2022). We determined a mean dissipation rate of 10.6

W/m^2 across 60 m between the two instruments, almost entirely due to bed friction (Figure 4 d).

317   Duce et al. (2022) recorded mean dissipation rates of 20 W/m^2 with wave heights of H$_s$ = 0.78 m and

318   T$_p$ = 5 seconds. Differences in the recoded and modelled data at this site may be attributed to the

319   incident wave direction (N-NE during the deployment period) which was not completely aligned with

320   SaG as modelled here. These results compare with data obtained on a fringing reef in Ipan (Guam)

321   which also featured SaG on the forereef (Péquignet et al., 2011). Between two sensors placed 55 m

322   apart inside a 5 m deep groove, the dissipation rate was 25 W/m^2 for offshore wave heights of 1-2 m

323   (Péquignet et al., 2011). Monismith et al. (2015) identified comparable dissipation rates of 25 W/m^2

324   on a forereef in Palmyra (Kiribati) between instruments 50 m apart for incident wave heights of 1 m.

325   Monismith et al. (2013) determined rates of 22 W/m^2 across a forereef at Mo'orea (French

326   Polynesia) with instruments located 50 m apart and wave heights of 0.3 to 0.5 m. Dissipation rates

327   for each of these studies are assumed to be due to bed friction with constant dissipation between

328   the instruments. Our results indicate that the dissipation rate across the forereef is heterogenous

329   and controlled by the bed morphology (e.g. Figure 5 a). The use of real bathymetries in modelling

330   efforts can elucidate the heterogeneity of dissipation rates on forereefs.

331   Using a real bathymetry, our study demonstrates the influence of groove sinuosity on wave energy

332   dissipation by breaking. Our results show that shore-normal waves interact with spur walls that do

333   not perfectly align with incoming swells. Indeed in our study, the mean groove heading was used to

334   align the bathymetric grids to the oncoming waves (Figure 2b), consistent with field observations

335   (Duce et al., 2020; Munk and Sargent, 1948). Despite this, variation in headings between grooves

336   and the sinuosity of individual grooves produces steep irregularities in the forereef slope that have a

337   large impact on the oncoming waves, playing a significant role on both dissipation by wave breaking

338   and bed friction. The straight and shore normal SaG identified in this analysis (mean sinuosity of

339   S=0.99, where 1 is a perfectly straight groove) (Table 4) are representative of groove sinuosity across

340   the southern Great Barrier Reef. For example, observations of 12,102 grooves in the GBR and South

341   Pacific show a mean groove sinuosity of S = 0.98 (Duce, 2017). Despite remarkable regional

342   consistency in groove morphology, we observed that even small deviations from perfect shore-

343   normal grooves are significant to wave transformation on the forereef. A more sensitive measure for

344   groove sinuosity may allow for a better understanding of forereef hydrodynamics. Further

345   investigation into SaG sinuosity effects should consider the natural sinuosity of SaG derived from

346   high resolution digital elevation models to account for these effects.

4.2 Effects of SaG from different morphological classes on wave energy dissipation

348   The most wave exposed site (southern site, OS) has the highest average dissipation rates of 71.5%

349   over 300 m SaG zone due to bed friction (Figure 4a). The long (mean length of 187.12 m) and deep

350   (mean depth of 1.95 m) exposed to wave energy (EWE) grooves at this exposed site may explain how

351   this high average dissipation rate occurred (Table 1). The length of EWE SaG creates surfaces of high

352   frictional drag that extend the zone of frictional dissipation and contribute to high average

353   dissipation rates (Figures 4a and 5). Shore normal currents occurring in the long and deep grooves

354   have also been observed and facilitate high rates of dissipation (Rogers et al., 2013). We

355   demonstrate under present-day conditions that bed frictional dissipation is dominant in dissipating

356   wave energy before breaking occurs at the reef crest (Figure 4a and c). Bed frictional dissipation

357   represents 98.0% and 98.9% of total dissipation at site OS and OE respectively (Figure 4a and c). This

358   is consistent with field research conducted at OTR (Duce et al., 2022) and in other high-energy

359   settings (Lowe et al., 2005; Monismith et al., 2015; Rogers et al., 2017). For example, under mean

360   wave conditions at Palmyra (Kiribati), a high bed friction coefficient (f_w =1.8) facilitated greater wave

361   energy dissipation due to bed friction than from wave breaking (Monismith et al., 2015), which is

362   consistent with field observations in Kaneohe Bay, Oahu, Hawaii (Lowe et al., 2005). Our results

363   suggest that the modes of wave energy dissipation (frictional or breaking) are not only influenced by

364   the wave conditions but also by the heterogenous morphology of the forereef slopes.

365   SaG morphology and consequently the morphological classes of Duce et al., (2016) can provide

366   further explanations to the mode of wave energy dissipation (Table 1). Where grooves are shorter,

367   they play a critical role in creating steep bathymetric gradients that induce wave breaking (Figures 4

368   and 8). This differs from previous SaG research (Acevedo-Ramirez et al., 2021) that showed wave

369   breaking being induced by the reef crest. Semi-exposed SaGs (represented here by site OE) are

370   typically shorter (mean length of 71.5 m) and shallower (mean depth of 1.38 m) than the most

371   exposed sites (site OS) and can include both exposed to wave energy (EWE) and deep and

372   disconnected (DaD) classes (Table 1). The seaward extent of the EWE grooves at semi-exposed

373   forereef sites (OE; Figure 4d) feature a steep bathymetric incline that produces the maximum wave

374   energy dissipation by wave breaking rate observed across all present-day models (1824.7 W/m^2,

375   Figure 5). As such, long spurs can facilitate frictional dissipation and short grooves can induce wave

376   breaking by introducing steep bathymetric inclines within the breaker zone of incident waves.
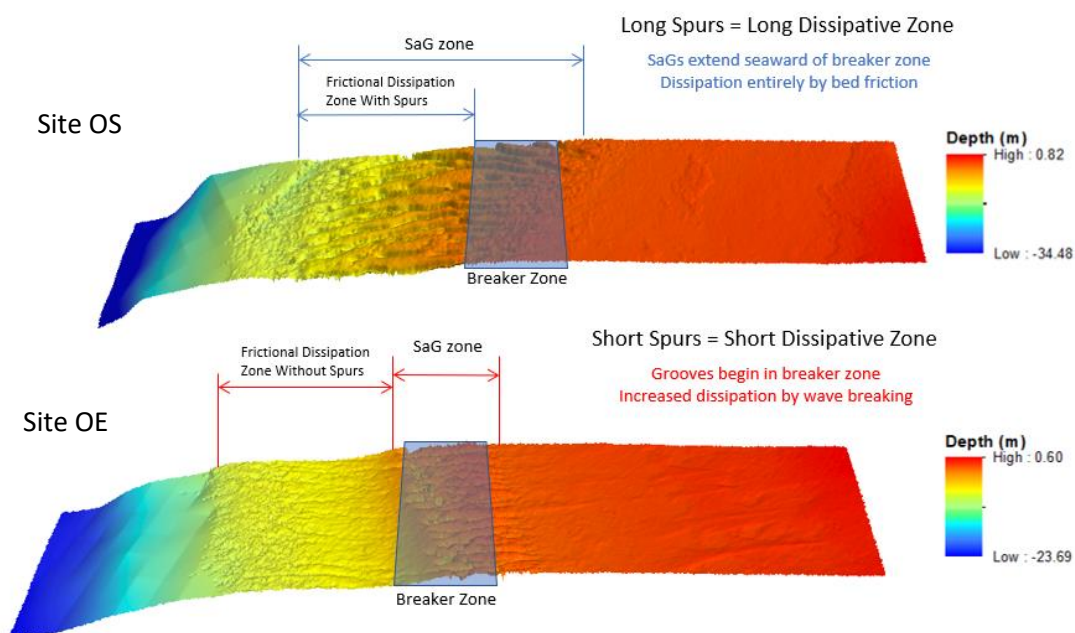

378   *Figure 8: A comparison between exposed and semi-exposed bathymetric profiles (site OS and site OE)*

379   *demonstrate the influence of the length of the SaG zone.*

380   The peak in wave energy dissipation at the shoreward of exposed to wave energy (EWE) grooves

381   highlights the complex interaction between forereef morphological evolution and wave energy

382   (Figure 4e). The seaward extent of EWE grooves is at a depth of 3.5 m, coincident with the mean

383   model wave height breaker depth for waves of 1.3 – 4.3 m (Figure 4, Table 2). As wave breaking

384   imposes forces on the structure of the reef (Massel & Gourlay, 2000; Storlazzi et al., 2005) the

385   results presented here suggest that incident waves could be capable of modifying the EWE grooves

386   in this zone, which is consistent with C14 and U-Th ages of SaG formations on the eastern forereef of

387   OTR (Duce et al., 2020), suggesting an erosive origin for this grooves. Imposed climate change effects

388   further elucidate the influence of grooves. Deep and disconnected (DaD) grooves at site OE exist

389   below the typical wave base and have minimal interaction with present day wave energy. Supporting

390   the previous findings that DaD grooves may be relict features, formed at an early stage during the

391   Holocene transgression (Duce et al., 2016).

4.3   The impact of climate change on wave energy dissipation over SaG

393   Forecasted environmental changes decrease mean wave energy dissipation (Figure 5) which is

394   consistent with other approaches (e.g., Quataert et al., 2015; Sheppard et al., 2005). In the

395   simulations presented here, dissipation remains high between RCP 2.6 and RCP 8.5 as reduced

396   dissipation by bed friction is balanced by an increase in dissipation by wave breaking (Figures 5 and

397   6). The difference between dissipation by bed friction and dissipation by wave breaking is the

398   greatest at both sites for RCP 8.5, where water depth is still sufficient for wave breaking, yet the

399   degradation of the reef reduces frictional effects (see Figure 9). A reliance on wave breaking

400   dissipation is consistent with observations from high energy reefs of low structural complexity

401   (Harris et al., 2018). Finally, dissipation is lowest where SLR is greatest (TD scenario) due to wave

402   passing over the reef without breaking (Figure 9). Although the role of SLR is thought to be

403   secondary in contributing to these changes (Harris et al., 2018), our models suggest that the

404   combined impact of SLR and loss of structural complexity will lead to lowest dissipation rates

405   (Figures 5 and 9) and highest wave overtopping (Figures 6 and 9) under future climate change

406   scenarios.

407   Sea-level rise (SLR) shifts the region of high energy dissipation toward the reef-crest (Figure 5b, c and

408   e, f). Bathymetric features that are submerged into the surf zone by rising relative sea level are likely

409   to influence wave breaking and frictional dissipation (Figure 5). This is evident in the shoreward

410   shifting dissipation zones (Figure 5) and as previous literature states (Massel and Gourlay, 2000) is a

411   threat to corals in this zone as wave breaking results in greater hydrodynamic forces on corals.

412   Corals previously protected from wave energy are likely to be species of lower mechanical strength

413   (Storlazzi et al., 2005). Under worse case scenarios (RCP 8.5) by the year 2100 it is likely that corals

414   of the same species may be weaker due to lower carbonate saturation in the water column (Eakin,

415   1996) or high frequency bleaching events (Hughes et al., 2017). Coral breakage is likely to occur here

416   and the corals that support a steep bathymetric incline with a high frictional coefficient responsible

417   for this peak in wave energy dissipation may have lower structural resilience by 2100 (Eakin, 1996).

418   High-energy SaG formations have been attributed to wave induced erosion, albeit at vastly different

419   timescales to sedimentary swash-zone features such as rip channels (Duce et al., 2020). It is possible

420   that climate change-driven increase in erosive forces promote further SaG development on

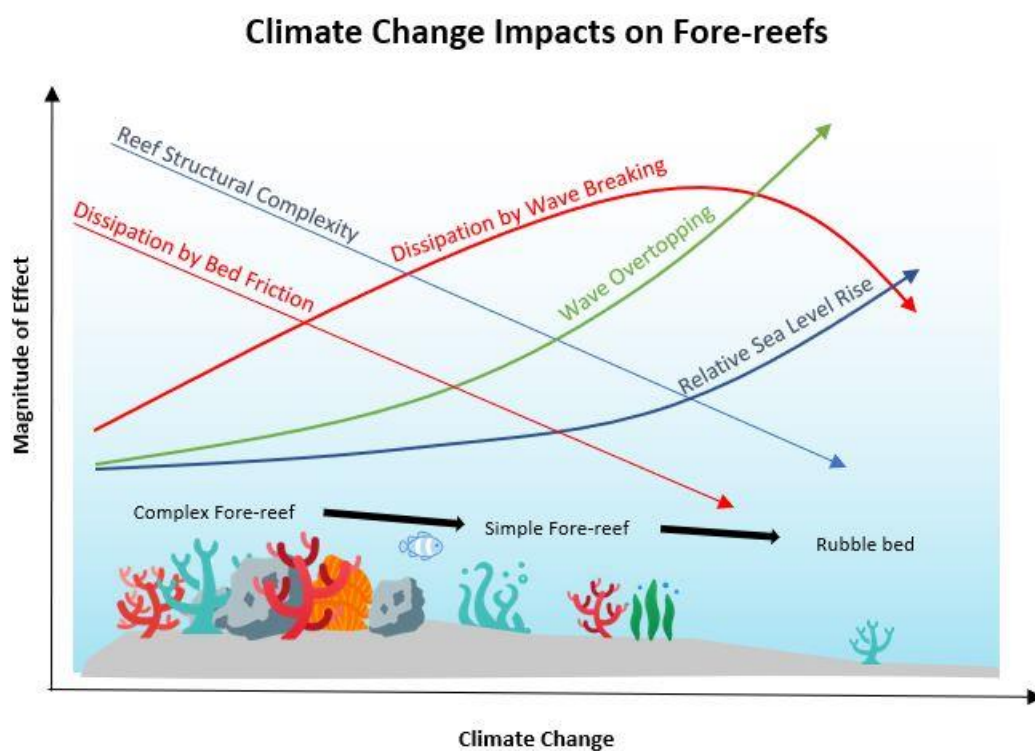421   forereefs, which contributes to the dissipation of wave energy.

422

423   *Figure 9: A conceptual diagram of changes to wave transformation on forereefs under increasing*

424   *climate change impacts. Climate driven inputs including loss of reef structural complexity and relative*

425   *sea-level rise are shown (blue). Dissipation rates (red) due to bed friction decreases, in response,*

426   *dissipation due to wave breaking increases until water depth exceeds breaker depths. Wave*

427   *overtopping (green) increases exponentially due to the combined effects of relative sea-level rise and*

428   *loss of reef structural complexity.*

429   ## 4.3.2 Potential for wave overtopping with climate change

430   Wave overtopping exponentially increases with climate change due to the coupled effects of

431   decreased bed friction and loss of dissipation due to breaking (Figure 7). Compared to mean wave

432   conditions, the impact of storm waves results in increasingly greater overtopping when climate

433   projections are increased. (Figure 7). This effect is persistent despite the increased wave energy

434   dissipation at the semi-exposed forereef (site OE) under RCP 8.5 (Figure 4e). The primary control on

435   wave overtopping is sea-level rise, which incorporates eustatic and local sources. Future work should

436   include tidal effects, which would contribute an additional 1.5 m of water level at mean spring high

437   tide at OTR (Harris et al., 2015). The magnitude of wave overtopping observed in the TD scenario at

438   the exposed site (OS) of ~4 m is sufficient to entirely flood all backreef environments at OTR,

439   including the low-lying coral island. This magnitude of wave overtopping would have significant

440   impacts on coral reef islands and reef-lined shores(Fellowes et al. 2022; Storlazzi et al. 2015;

441   Talavera et al. 2021). For example, 3.7 m of wave run up combined with sea surface elevation above

442   a reef flat in Roi-Namur, Marshall Islands, was observed in flooding of inland area of the Island

443   (Cheriton et al., 2016). Research elsewhere demonstrated that wave overtopping on reef islands in

444   the year 2100 will be highly variable across due to variable reef vertical accretion and erosion rates

445   (Beetham and Kench, 2018; Kench et al., 2022), but also due to the vertical accretion of coral reef

446   islands (Kench et al., 2019, 2022; Masselink et al., 2020) which is controlled by sediment availability.

447   The combined influence of coral reef degradation and sea-level rise amplifies the occurrence of

448   wave overtopping, thereby exposing communities located in the downwind direction of coral reefs

449   to heightened risks of flooding (Harris et al., 2018; Quataert et al., 2015; Storlazzi et al., 2018).

450   Notably, a maximum overtopping of approximately 4 m was measured here when the significant

451   wave height reached 5.1 m. An examination of altimeter data reveals that within the 33-year data

452   span, wave heights have not surpassed this threshold (95th percentile wave height = 3.1 m) (Figure

453   S1, supplementary material). Consequently, further investigation is required to determine the

454   frequency of significant overtopping events at OTR.

455   5. Conclusion

456   This study combined numerical modelling and LiDAR-derived bathymetry to demonstrate the

457   importance of forereef spur and groove (SaGs) morphologies in modifying wave energy. Results

458   indicate that high resolution digital elevation models (< 1 m) can provide morphometric data to

459   examine wave transformation on forereefs comparable to field studies. We show that groove

460   sinuosity plays a role in wave transformation and should be considered in future research on wave

461   dissipation on forereefs. This highlights the need for accurate bathymetries in future studies of

462   forereef wave energy dissipation, as idealized bathymetries used in previous studies, using

463   numerical or physical modelling, cannot provide results comparable to field studies.

464   We demonstrate that SaG morphological classes exhibit distinct dissipation characteristics, with

465   some showcasing higher frictional dissipation and others exhibiting greater breaking dissipation.

466   Notably, spur length emerges as a critical factor in enhancing dissipation by bed friction. Among the

467   SaG morphological classes, exposed to wave energy (EWE) grooves have demonstrated the most

468   substantial dissipation rates, while deep and disconnected (DaD) grooves contribute less to the

469   dissipation process, particularly evident under future climate change scenarios.

470   Projected climate change conditions may lead to a decrease in wave energy dissipation on forereefs.

471   Indeed, the climate change scenarios analysed demonstrated that changes in the mode of wave

472   energy dissipation will likely occur. The most notable result was a decrease in dissipation by bed

473   friction from 100% of dissipation under present day conditions to 48% under RCP 8.5. This is

474   matched by a 52% increase in dissipation by wave breaking. Overall, we found a loss in wave energy

475   dissipation under future climate change scenarios leading to increased wave overtopping, with the

476   maximum overtopping occurring where dissipation was lowest. Forereef morphological adjustment

477   to increased dissipation by wave breaking may expose corals to erosion, a process which has been

478   linked to the formation of SaG. The results highlight the critical role of forereef morphology in wave

479   energy dissipation and the need for measures to promote coral growth to facilitate future

480   dissipation. The findings have implications for the modelling wave transformation over forereefs to

481   provide insight into the future habitability of exposed reef-lined coasts.

482   ## 6. Acknowledgements

491   ## Data Availability

492

493   XBeach version 1.22 (revision 4567) is used in this analysis and can be accessed through a Docker

494   image available at https://hub.docker.com/r/tristansalles/docker2xbeach. Python codes used to

495   interpret LiDAR derived bathymetry in XBeach can be found at https://github.com/Lachie-

496   Perris/XBeach_coral. Satellite altimeter derived wave heights for the southern GBR are provided in

497   csv format with python notebooks at https://github.com/Lachie-Perris/RADWAVE_OTI.

498 References

499   Acevedo-Ramirez, César A., W. Stephenson, S. Wakes, and I. Mariño-Tapia. 2021. "Wave

500   Transformation on a Fringing Reef System With Spur and Groove Structures." *Journal of*

501   *Geophysical Research: Oceans* 126(9):1–14. doi: 10.1029/2020JC016910.

502   Amores, Angel, Marta Marcos, Gonéri Le Cozannet, and Jochen Hinkel. 2022. "Coastal Flooding and

503   Mean Sea-Level Rise Allowances in Atoll Island." *Scientific Reports* 12(1):1–12. doi:

504   10.1038/s41598-022-05329-1.

505   Baldock, T. E., A. Golshani, D. P. Callaghan, M. I. Saunders, and P. J. Mumby. 2014. "Impact of Sea-

506   Level Rise and Coral Mortality on the Wave Dynamics and Wave Forces on Barrier Reefs."

507   *Marine Pollution Bulletin* 83(1):155–64. doi: 10.1016/j.marpolbul.2014.03.058.

508   Baldock, T. E., Behnam Shabani, David P. Callaghan, Zhifang Hu, and Peter J. Mumby. 2020. "Two-

509   Dimensional Modelling of Wave Dynamics and Wave Forces on Fringing Coral Reefs." *Coastal*

510   *Engineering* 155. doi: 10.1016/j.coastaleng.2019.103594.

511   Beaman, R. J. 2017. "High-Resolution Depth Model for the Great Barrier Reef - 30 M."

512   Beetham, E., and P. S. Kench. 2018. "Predicting Wave Overtopping Thresholds on Coral Reef-Island

513   Shorelines with Future Sea-Level Rise." *Nature Communications* 9(1). doi: 10.1038/s41467-018-

514   06550-1.

515   Buckley, Mark L., Ryan J. Lowe, Jeff E. Hansen, and Ap R. Van Dongeren. 2016. "Wave Setup over a

516   Fringing Reef with Large Bottom Roughness." *Journal of Physical Oceanography* 46(8):2317–33.

517   doi: 10.1175/JPO-D-15-0148.1.

518   Buddemeier, R. W., and S. V. Smith. 1988. "Coral Reef Growth in an Era of Rapidly Rising Sea Level:

519   Predictions and Suggestions for Long-Term Research." *Coral Reefs* 7(1):51–56. doi:

520   10.1007/BF00301982.

521   Castillo, Karl D., Justin B. Ries, Jack M. Weiss, and Fernando P. Lima. 2012. "Decline of Forereef

522   Corals in Response to Recent Warming Linked to History of Thermal Exposure." *Nature Climate*

523   *Change* 2(10):756–60. doi: 10.1038/nclimate1577.

524   Cheriton, Olivia M., Curt D. Storlazzi, and Kurt J. Rosenberger. 2016. "Observations of Wave

525   Transformation over a Fringing Coral Reef and the Importance of Low-Frequency Waves and

526   Offshore Water Levels to Runup, Overwash, and Coastal Flooding." *Journal of Geophysical*

527   *Research: Oceans* 121(9):6762–78. doi: 10.1002/2016JC012132.Received.

528   De'Ath, Glenn, Katharina E. Fabricius, Hugh Sweatman, and Marji Puotinen. 2012. "The 27-Year

529   Decline of Coral Cover on the Great Barrier Reef and Its Causes." *Proceedings of the National*

530   *Academy of Sciences of the United States of America* 109(44):17995–99. doi:

531   10.1073/pnas.1208909109.

532   Dechnik, Belinda, Jody M. Webster, Peter J. Davies, Juan-carlos Braga, and Paula J. Reimer. 2015.

533   "Holocene ' Turn-on ' and Evolution of the Southern Great Barrier Reef : Revisiting Reef Cores

534   from the Capricorn Bunker Group." *Marine Geology* 363:174–90. doi:

535   10.1016/j.margeo.2015.02.014.

536   Duce, Stephanie. 2017. "The Form, Function and Evolution of Coral Reef Spurs and Grooves."

537   University of Sydney.

538   Duce, Stephanie, Belinda Dechnik, Jody M. Webster, Quan Hua, James Sadler, Gregory E. Webb, Luke

539   Nothdurft, Marcos Salas-Saavedra, and Ana Vila-Concejo. 2020. "Mechanisms of Spur and

540   Groove Development and Implications for Reef Platform Evolution." *Quaternary Science*

541   *Reviews* 231. doi: 10.1016/j.quascirev.2019.106155.

542   Duce, Stephanie, A. Vila-Concejo, S. M. Hamylton, J. M. Webster, E. Bruce, and R. J. Beaman. 2016.

543   "A Morphometric Assessment and Classification of Coral Reef Spur and Groove Morphology."

544   *Geomorphology* 265:68–83. doi: 10.1016/j.geomorph.2016.04.018.

545   Duce, Stephanie, A. Vila-Concejo, Sarah Hamylton, Eleanor Bruce, and Jody M. Webster. 2014. "Spur

546   and Groove Distribution, Morphology and Relationship to Relative Wave Exposure, Southern

547   Great Barrier Reef, Australia." *Journal of Coastal Research* 70:115–20. doi: 10.2112/si70-020.1.

548   Duce, Stephanie, A. Vila-Concejo, R. J. Mccarroll, B. Yiu, L. A. Perris, and J. M. Webster. 2022. "Field

549   Measurements from Contrasting Reefs Show Spurs and Grooves Can Dissipate More Wave

550   Energy than the Reef Crest." *Earth and Space Science Open Archive ESSOAr* 413(August

551   2021):108365. doi: 10.1016/j.geomorph.2022.108365.

552   Eakin, C. M. 1996. "Where Have All the Carbonates Gone? A Model Comparison of Calcium

553   Carbonate Budgets before and after the 1982–1983 El Nino at Uva Island in the Eastern

554   Pacific." *Coral Reefs* 15(2):109–19. doi: 10.1007/bf01771900.

555   Fellowes, Thomas E., Ana Vila-Concejo, Shari L. Gallop, Mitchell D. Harley, and Andrew D. Short.

556   2022. "Wave Shadow Zones as a Primary Control of Storm Erosion and Recovery on Embayed

557   Beaches." *Geomorphology* 399:108072. doi: 10.1016/j.geomorph.2021.108072.

558   Ferrario, F., M. W. Beck, C. D. Storlazzi, F. Micheli, C. C. Shepard, and L. Airoldi. 2014. "The

559   Effectiveness of Coral Reefs for Coastal Hazard Risk Reduction and Adaptation." *Nature

560   Communications* 5:3794. doi: 10.1038/ncomms4794.

561   Harris, Daniel L., Hannah E. Power, Michael A. Kinsela, Jody M. Webster, and Ana Vila-Concejo. 2018.

562   "Variability of Depth-Limited Waves in Coral Reef Surf Zones." *Estuarine, Coastal and Shelf

563   Science* 211(December 2016):36–44. doi: 10.1016/j.ecss.2018.06.010.

564   Harris, Daniel L., Alessio Rovere, Elisa Casella, Hannah Power, Remy Canavesio, Antoine Collin,

565   Andrew Pomeroy, Jody M. Webster, and Valeriano Parravicini. 2018. "Coral Reef Structural

566   Complexity Provides Important Coastal Protection from Waves under Rising Sea Levels."

567   *Science Advances* 4(2). doi: 10.1126/sciadv.aao4350.

568   Harris, Daniel L., A. Vila-Concejo, J. M. Webster, and H. E. Power. 2015. "Spatial Variations in Wave

569   Transformation and Sediment Entrainment on a Coral Reef Sand Apron." *Marine Geology*

570   363:220–29. doi: 10.1016/j.margeo.2015.02.010.

571   Harris, Daniel L., Jody M. Webster, Ana Vila-concejo, Stephanie Duce, and Javier X. Leon. 2023.

572   "Geomorphology Defining Multi-Scale Surface Roughness of a Coral Reef Using a High-

573   Resolution LiDAR Digital Elevation Model." *Geomorphology* 439(September 2022):108852. doi:

574   10.1016/j.geomorph.2023.108852.

575   Hughes, Terry P., James T. Kerry, Mariana Álvarez-Noriega, Jorge G. Álvarez-Romero, Kristen D.

576   Anderson, Andrew H. Baird, Russell C. Babcock, Maria Beger, David R. Bellwood, Ray

577   Berkelmans, Tom C. Bridge, Ian R. Butler, Maria Byrne, Neal E. Cantin, Steeve Comeau, Sean R.

578   Connolly, Graeme S. Cumming, Steven J. Dalton, Guillermo Diaz-Pulido, C. Mark Eakin, Will F.

579   Figueira, James P. Gilmour, Hugo Harrison, Scott F. Heron, Andrew S. Hoey, Jean Paul A. Hobbs,

580   mia O. Hoogenboom, Emma V Kennedy, Chao Yang Kuo, Janice M. Lough, ryan J. Lowe, Gang

581   Liu, Malcolm T. McCulloch, Hamish A. Malcolm, michael J. McWilliam, John M. Pandolfi, rachel

582   J. Pears, morgan S. Pratchett, Verena Schoepf, Tristan Simpson, William J. Skirving, Brigitte

583   Sommer, Gergely Torda, David R. Wachenfeld, Bette L. Willis, and Shaun K. Wilson. 2017.

584   "Global Warming and Recurrent Mass Bleaching of Corals." *Nature* 543(7645):373–77. doi:

585   10.1038/nature21707.

586   Hughes, Terry P., James T. Kerry, Andrew H. Baird, Sean R. Connolly, Andreas Dietzel, C. Mark Eakin,

587   Scott F. Heron, Andrew S. Hoey, Mia O. Hoogenboom, Gang Liu, Michael J. McWilliam, Rachel J.

588   Pears, Morgan S. Pratchett, William J. Skirving, Jessica S. Stella, and Gergely Torda. 2018.

589   "Global Warming Transforms Coral Reef Assemblages." *Nature* 556(7702):492–96. doi:

590   10.1038/s41586-018-0041-2.

591   Jell, John S., and Gregory E. Webb. 2012. "Geology of Heron Island and Adjacent Reefs, Great Barrier

592   Reef, Australia." *Episodes* 35(1):110–19. doi: 10.18814/epiiugs/2012/v35i1/010.

593   Kench, Paul S., Edward P. Beetham, Tracey Turner, Kyle M. Morgan, Susan D. Owen, and Roger. F.

594   McLean. 2022. "Sustained Coral Reef Growth in the Critical Wave Dissipation Zone of a

595   Maldivian Atoll." *Communications Earth & Environment* 3(1):1–12. doi: 10.1038/s43247-021-

596   00338-w.

597   Kench, Paul S., Murray R. Ford, and Susan D. Owen. 2019. "Patterns of Island Change and Persistence

598   Offer Alternate Adaptation Pathways for Atoll Nations." *Nature Communications* 9(1). doi:

599   10.1038/s41467-018-02954-1.

600   Knutson, Thomas R., Joseph J. Sirutis, Ming Zhao, Robert E. Tuleya, Morris Bender, Gabriel A. Vecchi,

601   Gabriele Villarini, and Daniel Chavas. 2015. "Global Projections of Intense Tropical Cyclone

602   Activity for the Late Twenty-First Century from Dynamical Downscaling of CMIP5/RCP4.5

603   Scenarios." *Journal of Climate* 28(18):7203–24. doi: 10.1175/JCLI-D-15-0129.1.

604   Lashley, Christopher H., Dano Roelvink, Ap van Dongeren, Mark L. Buckley, and Ryan J. Lowe. 2018.

605   "Nonhydrostatic and Surfbeat Model Predictions of Extreme Wave Run-up in Fringing Reef

606   Environments." *Coastal Engineering* 137(October 2017):11–27. doi:

607   10.1016/j.coastaleng.2018.03.007.

608   Lowe, R. J., J. L. Falter, M. D. Bandet, G. Pawlak, M. J. Atkinson, S. G. Monismith, and J. R. Koseff.

609   2005. "Spectral Wave Dissipation over a Barrier Reef." *J. Geophys. Res* 110:4001. doi:

610   10.1029/2004JC002711.

611   Madin, Joshua S., and Sean R. Connolly. 2006. "Ecological Consequences of Major Hydrodynamic

612   Disturbances on Coral Reefs." *Nature* 444(7118):477–80. doi: 10.1038/nature05328.

613   Massel, S. R., and M. R. Gourlay. 2000. "On the Modelling of Wave Breaking and Set-up on Coral

614   Reefs." *Coastal Engineering* 39(1):1–27. doi: 10.1016/S0378-3839(99)00052-6.

615   Masselink, Gerd, Eddie Beetham, and Paul Kench. 2020. "Coral Reef Islands Can Accrete Vertically in

616   Response to Sea Level Rise." *Sci. Adv* 6(June):3656–66.

617   Meucci, Alberto, Ian R. Young, Mark Hemer, Ebru Kirezci, and Roshanka Ranasinghe. 2020.

618   "Projected 21st Century Changes in Extreme Wind-Wave Events." *Science Advances*

619   6(24):7295–7305. doi: 10.1126/sciadv.aaz7295.

620   Monismith, Stephen G., Liv M.M. Herdman, Soeren Ahmerkamp, and James L. Hench. 2013. "Wave

621   Transformation and Wave-Driven Flow across a Steep Coral Reef." *Journal of Physical*

622   *Oceanography* 43(7):1356–79. doi: 10.1175/JPO-D-12-0164.1.

623   Monismith, Stephen G., Liv M. M. Herdman, Soeren Ahmerkamp, and James L. Hench. 2013. "Wave

624   Transformation and Wave-Driven Flow across a Steep Coral Reef." *Journal of Physical*

625   *Oceanography* 43(7):1356–79. doi: 10.1175/JPO-D-12-0164.1.

626   Monismith, Stephen G., Justin S. Rogers, David Koweek, and Robert B. Dunbar. 2015. "Frictional

627   Wave Dissipation on a Remarkably Rough Reef." *Geophysical Research Letters* 42(10):4063–71.

628   doi: 10.1002/2015GL063804.

629   Montaggioni, Lucien F. 2005. "History of Indo-Pacific Coral Reef Systems since the Last Glaciation:

630   Development Patterns and Controlling Factors." *Earth-Science Reviews* 71(1–2):1–75. doi:

631   10.1016/j.earscirev.2005.01.002.

632   Munk, Walter H., and Martson C. Sargent. 1948. "Adjustment of Bikini Atoll to Ocean Waves."

633   *Transactions, American Geophysical Union* 29(6):855. doi: 10.1029/TR029i006p00855.

634   Osorio-Cano, Juan D., Juan C. Alcérreca-Huerta, Andrés F. Osorio, and Hocine Oumeraci. 2018. "CFD

635   Modelling of Wave Damping over a Fringing Reef in the Colombian Caribbean." *Coral Reefs*

636   37(4):1093–1108. doi: 10.1007/s00338-018-1736-4.

637   Pepper, A., and M. L. Puotinen. 2009. "Gremo: A GIS-Based Generic Model for Estimating Relative

638   Wave Exposure." *18th World IMACS Congress and MODSIM 2009 - International Congress on*

639   *Modelling and Simulation: Interfacing Modelling and Simulation with Mathematical and*

640   *Computational Sciences, Proceedings* 1964–70.

641   Péquignet, A. C., J. M. Becker, M. A. Merrifield, and S. J. Boc. 2011. "The Dissipation of Wind Wave

642   Energy across a Fringing Reef at Ipan, Guam." *Coral Reefs* 30(SUPPL. 1):71–82. doi:

643   10.1007/s00338-011-0719-5.

644   Péquignet, Anne-Christine N., Janet M. Becker, and Mark A. Merrifield. 2014. "Energy Transfer

645   between Wind Waves and Low-Frequency Oscillations on a Fringing Reef, Ipan, Guam." *Journal*

646   *of Geophysical Research: Oceans* 119(10):6709–24. doi: 10.1002/2014JC010179.

647   Perry, Chris T., Lorenzo Alvarez-Filip, Nicholas A. J. Graham, Peter J. Mumby, Shaun K. Wilson, Paul S.

648   Kench, Derek P. Manzello, Kyle M. Morgan, Aimee B. A. Slangen, Damian P. Thomson, Fraser

649   Januchowski-Hartley, Scott G. Smithers, Robert S. Steneck, Renee Carlton, Evan N. Edinger, Ian

650   C. Enochs, Nuria Estrada-Saldívar, Michael D. E. Haywood, Graham Kolodziej, Gary N. Murphy,

651   Esmeralda Pérez-Cervantes, Adam Suchley, Lauren Valentino, Robert Boenish, Margaret

652   Wilson, and Chancey MacDonald. 2018. "Loss of Coral Reef Growth Capacity to Track Future

653   Increases in Sea Level." *Nature* 558(7710):396–400. doi: 10.1038/s41586-018-0194-z.

654   Quataert, Ellen, Curt Storlazzi, Ap van Dongeren, and Robert McCall. 2020. "The Importance of

655   Explicitly Modelling Sea-Swell Waves for Runup on Reef-Lined Coasts." *Coastal Engineering*

656   160(April):103704. doi: 10.1016/j.coastaleng.2020.103704.

657   Quataert, Ellen, Curt Storlazzi, Arnold Van Rooijen, Olivia Cheriton, and Ap Van Dongeren. 2015a.

658   "The Influence of Coral Reefs and Climate Change on Wave-Driven Flooding of Tropical

659   Coastlines." *Geophysical Research Letters* 42(15):6407–15. doi: 10.1002/2015GL064861.

660   Quataert, Ellen, Curt Storlazzi, Arnold Van Rooijen, Olivia Cheriton, and Ap Van Dongeren. 2015b.

661   "The Influence of Coral Reefs and Climate Change on Wave-Driven Flooding of Tropical

662   Coastlines." *Geophysical Research Letters* 42(15):6407–15. doi: 10.1002/2015GL064861.

663   Reguero, Borja G., Iñigo J. Losada, and Fernando J. Méndez. 2019. "A Recent Increase in Global Wave

664   Power as a Consequence of Oceanic Warming." *Nature Communications* 10(1):1–14. doi:

665   10.1038/s41467-018-08066-0.

666   Roelvink, Dano, A. Reniers, Ap van Dongeren, J. S. M. van Thiel de Vries, J. Lescinski, and R. T. McCall.

667   2015. *XBeach Model Description and Manual*.

668   Rogers, Justin S., Stephen G. Monismith, Falk Feddersen, and Curt D. Storlazzi. 2013.

669   "Hydrodynamics of Spur and Groove Formations on a Coral Reef." *Journal of Geophysical*

670   *Research: Oceans* 118(6):3059–73. doi: 10.1002/jgrc.20225.

671   Rogers, Justin S., Stephen G. Monismith, Oliver B. Fringer, David A. Koweek, and Robert B. Dunbar.

672   2017. "A Coupled Wave-Hydrodynamic Model of an Atoll with High Friction: Mechanisms for

673   Flow, Connectivity, and Ecological Implications." *Ocean Modelling* 110. doi:

674   10.1016/j.ocemod.2016.12.012.

675   Rogers, Justin S., Stephen G. Monismith, David A. Koweek, and Robert B. Dunbar. 2016. "Wave

676   Dynamics of a Pacific Atoll with High Frictional Effects." *Journal of Geophysical Research:*

677   *Oceans* 121(1):350–67. doi: 10.1002/2015JC011170.

678   Sanborn, Kelsey L., Jody M. Webster, Gregory E. Webb, Juan Carlos Braga, Marc Humblet, Luke

679   Nothdurft, Madhavi A. Patterson, Belinda Dechnik, Susan Warner, Trevor Graham, Richard J.

680   Murphy, Yusuke Yokoyama, Stephen P. Obrochta, Jian xin Zhao, and Marcos Salas-Saavedra.

681   2020. "A New Model of Holocene Reef Initiation and Growth in Response to Sea-Level Rise on

682   the Southern Great Barrier Reef." *Sedimentary Geology* 397:105556. doi:

683   10.1016/j.sedgeo.2019.105556.

684   Saunders, Megan I., Simon Albert, Chris M. Roelfsema, Javier X. Leon, Colin D. Woodroffe, Stuart R.

685   Phinn, and Peter J. Mumby. 2016. "Tectonic Subsidence Provides Insight into Possible Coral

686   Reef Futures under Rapid Sea-Level Rise." *Coral Reefs* 35(1):155–67. doi: 10.1007/s00338-015-

687   1365-0.

688   Sheppard, Charles. 1981. "The Groove and Spur Structures of Chagos Atolls and Their Coral

689   Zonation." *Estuarine, Coastal and Shelf Science* 12(5):549–60. doi: 10.1016/S0302-

690   3524(81)80081-3.

691   Sheppard, Charles, David J. Dixon, Michael Gourlay, Anne Sheppard, and Rolph Payet. 2005. "Coral

692   Mortality Increases Wave Energy Reaching Shores Protected by Reef Flats: Examples from the

693   Seychelles." *Estuarine, Coastal and Shelf Science* 64(2–3):223–34. doi:

694   10.1016/j.ecss.2005.02.016.

695   Shinn, Eugene. 1963. "Spur and Groove Formation on the Florida Reef Tract." *SEPM Journal of*

696   *Sedimentary Research* Vol. 33(2):291–303. doi: 10.1306/74d70e34-2b21-11d7-

697   8648000102c1865d.

698   Shukla, P. R., J. Skea, R. Slade, R. van Diemen, E. Haughey, J. Malley, M. Pathak, and J. Portugal

699   Pereira. 2019. *IPCC, 2019: Technical Summary*.

700   Shukla, P. R., J. Skea, R. Slade, R. van Diemen, E. Haughey, J. Malley, M. Pathak, and J. Portugal

701   Pereira. 2019. *IPCC, 2019: Technical Summary*.

702   da Silva, Renan F., Curt D. Storlazzi, Justin S. Rogers, Johan Reyns, and Robert McCall. 2020.

703   "Modelling Three-Dimensional Flow over Spur-and-Groove Morphology." *Coral Reefs*. doi:

704   10.1007/s00338-020-02011-8.

705   Smith, Courtney, Tristan Salles, and Ana Vila-Concejo. 2022. "Offshore Wave Climate of the Great

706   Barrier Reef." *In Review* (0123456789). doi: 10.1007/s00338-023-02377-5.

707   Smith, Courtney, Ana Vila-Concejo, and T. B. Salles. 2020. "RADWave: Python Code for Ocean

708   Surface Wave Analysis by Satellite Radar Altimeter." *Journal of Open Source Software* 1(5):46.

709   doi: https://doi.org/10.21105/joss.02083.

710   Smyth, C., and Alex A. Hay. 2002. "Wave Friction Factors in Nearshore Sands." *Journal of Physical*

711   *Oceanography* 32(12):3490–98. doi: 10.1175/1520-0485(2002)032<3490:WFFINS>2.0.CO;2.

712   Sous, Damien, Samantha Maticka, Samuel Meulé, and Frédéric Bouchette. 2022. "Bottom Drag

713   Coefficient on a Shallow Barrier Reef." *Geophysical Research Letters* 1–12. doi:

714   10.1029/2021gl097628.

715   Storlazzi, C. D., E. K. Brown, M. E. Field, K. Rodgers, and P. L. Jokiel. 2005. "A Model for Wave Control

716   on Coral Breakage and Species Distribution in the Hawaiian Islands." *Coral Reefs* 24(1):43–55.

717   doi: 10.1007/s00338-004-0430-x.

718   Storlazzi, Curt D., Edwin P. L. Elias, and Paul Berkowitz. 2015. "Many Atolls May Be Uninhabitable

719   Within Decades Due to Climate Change." *Scientific Reports* 5(1):1–9. doi: 10.1038/srep14546.

720   Talavera, Lara, Ana Vila-Concejo, Jody M. Webster, Courtney Smith, Stephanie Duce, Thomas E.

721   Fellowes, Tristan Salles, Daniel Harris, Jon Hill, Will Figueira, and Jörg Hacker. 2021.

722   "Morphodynamic Controls for Growth and Evolution of a Rubble Coral Island." *Remote Sensing*

723   13(8):1–23. doi: 10.3390/rs13081582.

724   Yao, Yu, Yicheng Liu, Long Chen, Zhengzhi Deng, and Changbo Jiang. 2020. "Study on the Wave-

725   Driven Current around the Surf Zone over Fringing Reefs." *Ocean Engineering* 198. doi:

726   10.1016/j.oceaneng.2020.106968.

727   Young, I. R. 1992. "The Determination of Spectral Parameters from Significant Wave Height and Peak

728   Period." *Ocean Engineering* 19(5):497–508. doi: 10.1016/0029-8018(92)90008-R.

729

Supporting Information for

The influence of coral reef spur and groove morphology on wave energy dissipation and wave overtopping under future climate change scenarios

Lachlan Perris[1,*], Tristan Salles [1], Thomas E Fellowes[1], Stephanie Duce[2], Jody Webster[1], Ana Vila-Concejo[1]

[1] Geocoastal Research Group and Marine Studies Institute, School of Geosciences, The University of Sydney, NSW, 2006, Australia
[2] College of Science and Engineering, James Cook University, Bebegu Yumba Campus, Townsville, Queensland 4811, Australia

Contents of this file

Introduction

We determined mean offshore wave conditions near One Tree Reef (OTR) in the southern Great Barrier Reef. Satellite altimeter observations over 30 years (1985–2015) were obtained with RADWave (Smith et al., 2020). A small region (0.6° x 0.4°) representing dense altimeter data tracks was identified on the eastern, exposed side of OTR (Figure S1).
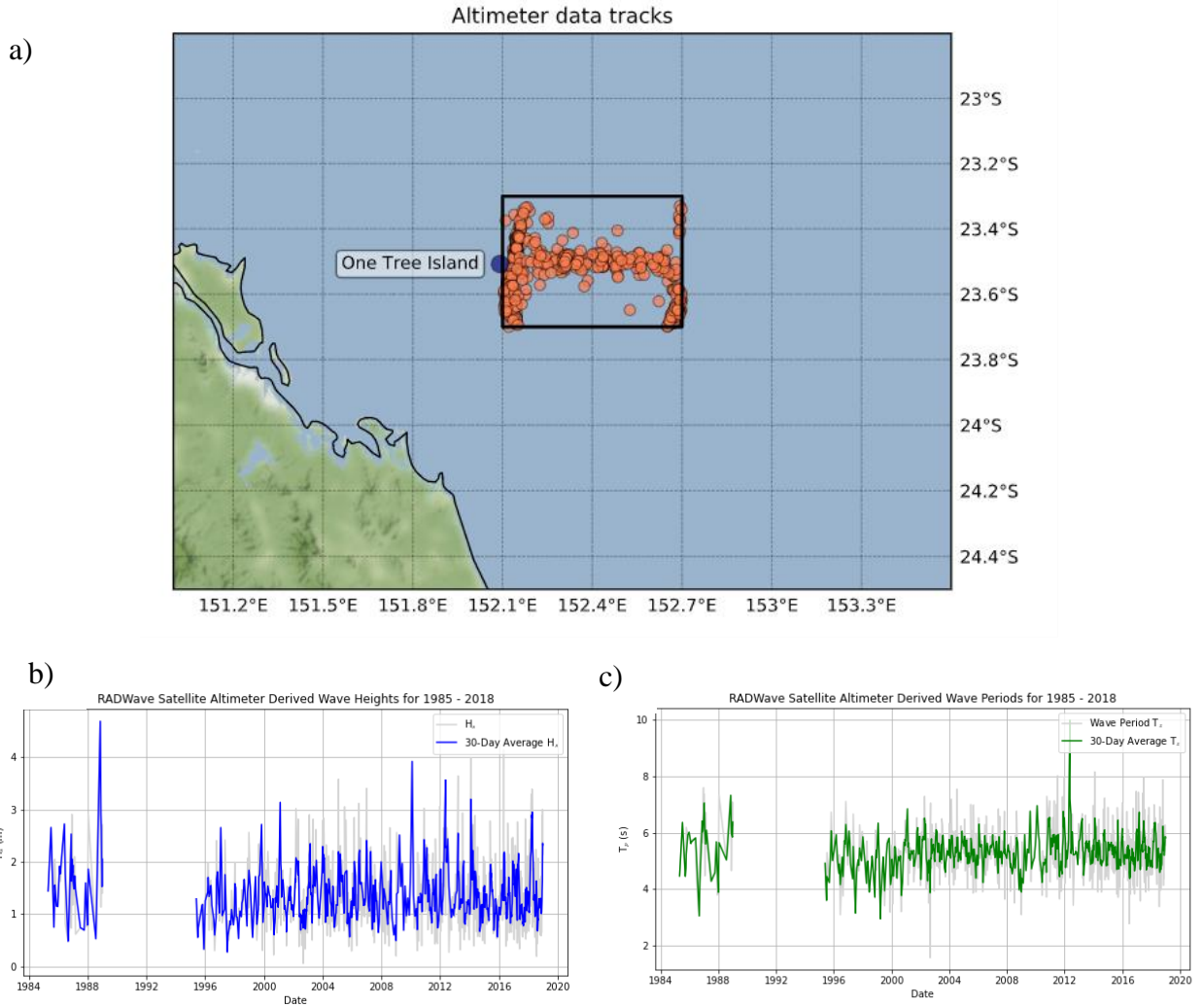
Figure S1. Altimeter data is extracted from the eastern (open ocean) side of OTR. Mean significant wave height across the 33-year study period was 1.34 m with a mean wave period of 5.2 seconds. A maximum wave height of 4.8 m.